修 士 論 文

Positioning Accuracy Improvement in Urban Area using multi-GNSS, Sophisticated Multipath Correlator and Improved Ray-tracing

(都心部におけるマルチ GNSS、高度マルチパスコリレータとレイトレーシングを用いての測位精度向上)

指導教員　上條 俊介 准教授

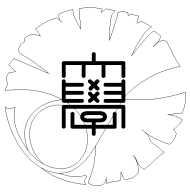

東京大学大学院
情報理工学系研究科
電子情報学専攻

学籍番号・氏名　48–136451 陳 飛宇

提出日　2015 年 2 月 5 日

概要

The most reliable solution for positioning in outdoor environment is using satellite-based positioning systems like GPS and GLONASS. In urban area, however, signals from some satellites will be reflected by tall buildings and thus cause positioning error. Although these satellites can be detected and eliminated from calculation through ray-tracing, this will also cause the insufficiency of usable satellites. To solve this problem, we combine the ray-tracing method and multi-GNSS method together to increase the number of usable satellites and positioning accuracy. Besides, the combination, a more sophisticated multipath correlation envelope is develop based on the material of the reflect surface. And to the cases of some deep urban environment where both one time reflection and the second time reflection could happen, a upgraded algorithm has been developed to detected the second time reflection. Experiments are conducted at Hitotsubashi area of Tokyo to prove effectiveness of the proposed methods.

目次

図目次

表目次

第 1 章

Introduction

This research focuses on improving positioning accuracy of satellite-based positioning method in urban area using 3D map and improved ray-tracing algorithm. Compared with the conventional method, the new method proposed in this research is able to give more accurate results in various scenarios. This chapter includes research background, research purposes and the organization of this thesis.

1.1 Background

Position information is becoming more and more crucial currently. Numerous applications require precise position information, usually 1m in accuracy, in order to provide advanced services. In big cities, especially downtown areas, accurate position information is required by all kinds of applications such as shop recommending, pedestrian counting, navigation and autonomous driving.

GPS, as the most developed satellite-based positioning system in the world, has been wildly used in all kinds of devices and applications. GPS is capable of providing reliable position information in most cases, and is also able to calculate 3-dimension position based on Earth-Centre-Earth-Fixed (ECEF) coordinates, which is extremely helpful in the research. There are many kinds of positioning methods based on GPS satellites, for instance, D-GPS (Differential-GPS uses several base stations to facilitate the positioning), A-GPS (Assisted-GPS is designed for mobile terminal use) and PPP (Precise Point Positioning uses signal frequency instead of distance to position). In this paper, the very basic GPS method is used and its positioning principle is illustrated in Fig. 1.1

Theoretically, 3 satellites are needed to calculate a position, but because the GPS system and receiver both have a clock offset, 4 satellites are needed for the positioning.

Currently, most smart phones and navigation devices have commercial level GPS receivers built inside and are able to output position within 10m accuracy. In vehicle scenario, GPS can be combined with other sensors like Gyro and steel wheel to output

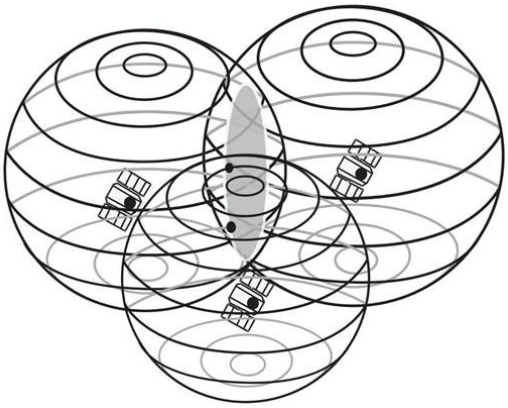

図 1.1: The fundamental principle of GPS

more accurate, which means that gaining vehicle position in urban area can be quite easy. In pedestrian scenario, however, the position information is not easy to calculate because firstly, there are no additional sensor for pedestrians and secondly, the movement of human is very random and hard to predict. Besides, GPS signals can be blocked by skyscrapers in urban area and even those received by pedestrians can be reflected by building surfaces and thus unreliable.

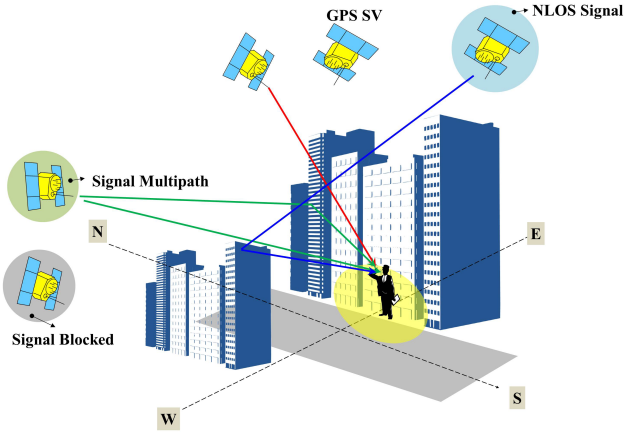

図 1.2: Possible GPS signal propagations in urban area

To illustrate, Fig. **??** shows several possible way for GPS signal to propagate. The red line denotes the line-of-sight (LOS) signal, which is not effected by buildings and thus reliable. The blue ray is non-line-of-sight signal, which means that the signal is transmitted from an invisible satellite and it reaches the receiver through reflection. Those reflected signals contain a lot of error and thus should not be trusted. The green ray denotes the multipath signal. This signal also has errors because the LOS signal and the reflected signal reach a receiver in a very short interval and hence the LOS signal is degraded. To solve this problem, a sophisticated material-based multipath correlation

envelop is developed. In addition to LOS, NLOS and multipath, many satellites, marked as BLOCKED in Fig. 1.2, are blocked by the tall buildings so that even reflected signals can not reach receiver. And if the total number of signal-reachable satellites is below 4, the positioning with GPS will not be possible. Normally, the position error in urban area will be around 50m, and even above 100m in deep urban area.[1]

図 1.3: Conventional GPS result in urban area

Fig. 1.3 shows the ground truth (cyan line) and the common result of conventional GPS and the ground truth (green dot). As can be observed, most of the points of convention GPS locate on the opposite side of the road and even in the intersection, the result also suffers a lot from the signal reflection. The average error in this case is around 25m.

In conclusion, getting position information using satellite-based method in urban area is still very difficult and the information is extremely valuable to many applications. Hence, upgrading the positioning accuracy answers for many actual social needs.

1.2 Research Purpose

According to [2] and illustrated by Fig. 1.4, the number of LOS satellites in urban area is below 4 at most of the time, which means no reliable result can be calculated at the most of the time.

In order to solve this problem, Miura Shunsuke used 3D map and ray tracing method

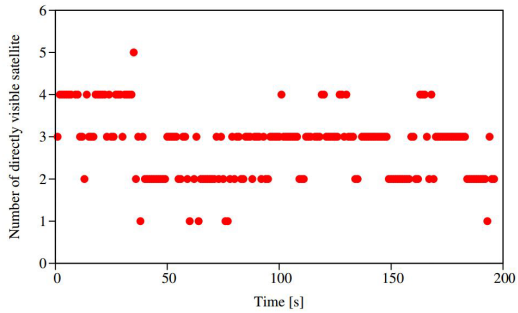

図 1.4: Number of LOS GPS satellites in urban area

to detect and use NLOS satellites to increase the usable number of satellites. [3] also points out that besides GPS and GLONASS, the Quasi-Zenith Satellites System (QZSS) of Japan, Beidou of China and Galileo of Europe are currently being developed and the method that uses all of these constellations (multi-GNSS) is expected to solve the satellite insufficient problem in urban area in 2020.

In addition to the problem mentioned above, there is also another problem called multipath. Multipath happens when both a LOS signal and a reflected signal from the same satellite reach at the receiver in very short interval, as illustrated in Fig. 1.2.

Moreover, to some specific deep urban environment, an improved ray tracing algorithm is proposed - the second time reflection algorithm. The detail of the algorithm will be introduced in the following chapters.

In conclusion, this thesis focuses on improving the pedestrian positioning accuracy in urban area through the following 3 aspects:

1) Increase the total number of satellites on the orbit by combining GPS and GLONASS together.
2) Correct multipath bias using a reflection surface mater-based multipath correlation envelop.
3) Improve ray tracing algorithm to detect the second time reflection in deep urban environment.

1.3 Thesis Structure

The structure of this paper is listed as follow.

In chapter 2 the basic concept of GPS and Miura's 3D map and ray tracing method is introduced.

In chapter 3 the fundamental knowledge about GPS system and 3D map ray tracing method is presented.

In chapter 4 the multipath error and the multipath correlator, a way to mitigate the error, and material-based multipath correlator is proposed.

In chapter 5 an improved ray tracing algorithm, the double reflection algorithm, is tested.

In the end, chapter 6 presents the conclusion and future works concerning this research.

第 2 章

GPS System and Related Researches

GPS is short for Global Positioning System. GPS is initially developed by America in 1973 and various kinds of researches have been done in this field. Currently, there are several ways of using GPS signal to calculate positions, and in this thesis the method of using distance (pseudorange) and the least weight square algorithm is researched.

In this chapter, a brief introduction of the GPS fundamental, the reasons for positioning bias and a improved positioning algorithm based on which this thesis is composed are presented.

2.1 GPS Fundamentals

GPS is originally designed to provide position, speed and time information with high accuracy for military purposes. Thanks to its high reliability and global coverage, GPS has been opened to public and now GPS is the mainly source for position information worldwide and basically every airplane, vehicle and mobile device has a GPS receiver built inside to provide customers with position information.

Since 1973, the beginning of GPS project, there has been 32 GPS satellites launched into the space and covers the whole planet. Besides American GPS, there are other Global Navigation Satellite Systems exist or being developed. For instance, Russian GLONASS which has 24 satellites, China BeiDou Navigation Satellite System, European Union's GALILEO are currently being developed. In addition to GNSS, Regional Navigation Satellite System (RNSS) is also a focus of many countries. The most typical one is Quasi-Zenith Satellite System (QZSS) of Japan. This system covers Japan, parts of Asia and Australia.

By the time of 2020, all the navigation satellite systems will be fully developed and the overall satellites in the orbit will be around 80, which means the position information will be much more easy to get and more accurate in the future.

2.1.1 Positioning Principles

GPS is composed of 3 parts - the space segments include satellites and satellite launchers, the control segments include include several monitor stations around the world and user segments. Fig. 2.1 illustrates the system.

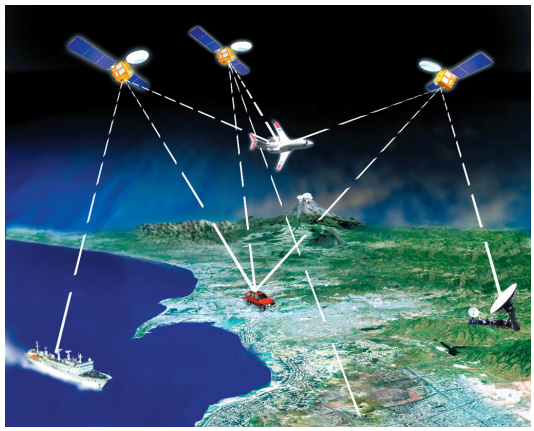

図 2.1: Composition of GPS: Space segment(satellites), Control segment(monitor stations) and users

Fig. 2.2 denotes the positioning principle of GPS. GPS uses the law of trilateration to calculate a position. Assuming that the coordinates of the satellites (center of a sphere) are known and the distances between a receiver and the satellites are also known, then three spheres can be drawn, as illustrated in Fig. 2.2. If only considering sphere 1 and sphere 2, a circle, colored in pink, can be found and with sphere 3, 2 points, colored in yellow, can be fixed. Usually, the coordinates of these two points should be one near the surface of the planet earth and the other one in the space, as a result, the receiver just need to find the reasonable one and output to the user.

Theoretically, GPS is valid when signals from three different satellites can be received by a receiver. In reality, however, signals from at least four satellites should be observed by a receiver in order for it to output a reliable position. The reason for this is because the receiver calculates the distances between itself and GPS satellites using signal propagation time, and in order to get the time, clocks are built inside of the receiver and the GPS satellites and there are offsets for the clocks [4]. Since the offsets of the GPS satellites can be calculated based on the "Ephemeris" informations sent by the satellites, but the receiver clock offset has no way to be calculated and is too big to be ignored. Hence, four satellites are required to calculate a receiver position along with a receiver clock bias.

The algorithm used in the position calculation is named the least squares method. The formulas are listed as follow:

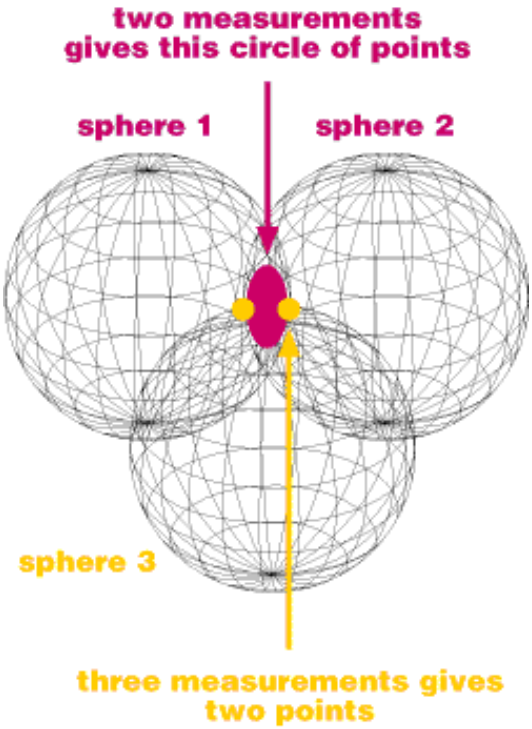

図 2.2: GPS uses trilateration theory to positioning

$$r_1 = \sqrt{(\alpha_1 - x)^2 + (\beta_1 - y)^2 + (\gamma_1 - z)^2} + s$$
$$r_2 = \sqrt{(\alpha_2 - x)^2 + (\beta_2 - y)^2 + (\gamma_2 - z)^2} + s$$
$$r_3 = \sqrt{(\alpha_3 - x)^2 + (\beta_3 - y)^2 + (\gamma_3 - z)^2} + s$$
$$r_4 = \sqrt{(\alpha_4 - x)^2 + (\beta_4 - y)^2 + (\gamma_4 - z)^2} + s$$

In the formulas, (α, β, γ) are the coordinates of the 4 satellites, which can also be calculated using the "Ephemeris" information, the (x,y,z) are the receiver's coordinates and s is the receiver's clock offset and r are the 4 distances from the satellites.

The distances from the satellites are defined as "pseudorange" and is computed by using the propagation time calculated based on the time the signal is sent and the time the signal is received. However, as discussed above, the receiver time is not synchronized with GPS system time and hence the distances computed using that time to multiply the speed of light are different with the true geometric distance.

For instance, if a signal from satellite n arrived at the receiver at GPS time t, and supposingly the signal propagation time is τ, then the time when the signal was sent is $t^{\mathrm{sv}}(t - \tau)$ and the time when the receiver receive the signal is $t^{\mathrm{r}}(t)$. According to this premise, the formula to calculate this pseudorange is:

$$\rho_n(t) = c\,[t^{\mathrm{r}}(t) - t_n^{\mathrm{SV}}(t-\tau)]$$

In the formula above, t and τ are both unknown. And the relationship of receiver time $t^{\mathrm{r}}(t)$ and satellite time $t_n^{\mathrm{SV}}(t-\tau)$ is like:

$$t^{\mathrm{r}}(t) = t + \delta t^{\mathrm{r}}(t)$$

$$t_n^{\mathrm{SV}}(t-\tau) = (t-\tau) + \delta t_n^{\mathrm{SV}}(t-\tau)$$

In the formulas above, $\delta t^{\mathrm{r}}(t)$ is the receiver clock with GPS time correction, $\delta t_n^{\mathrm{SV}}(t)$ is the satellite clock with GPS time correction. Considering this, the psudorange computation formula should be:

$$\rho_n(t) = c\,[t + \delta t^{\mathrm{r}}(t) - ((t-\tau) + \delta t_n^{\mathrm{SV}}(t-\tau))] + \varepsilon(t) = c\tau + c\,[\delta t^{\mathrm{r}}(t) - \delta t_n^{\mathrm{SV}}(t-\tau)] + \varepsilon(t)$$

In this formula, ε means the errors that can not be modeled. And Fig. 2.3 denotes the relationship.

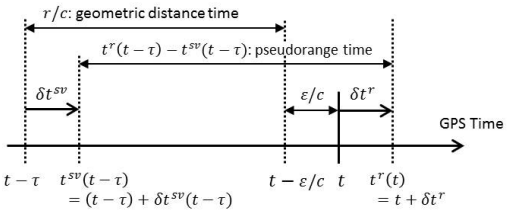

図 2.3: The explanation of time relationships in GPS

Moreover, pseudorange can be displayed as

$$r_n(t, t-\tau) = c\tau - I_n(t) - T_n(t)$$

where $I_n(t)$ and $T_n(t)$ denote ionosphere and troposphere delay which happen when signal penetrate the earth atmosphere. In this way, the formula for the pseudorange computation should be:

$$\rho_n = r_n + c\,[\delta t^{\mathrm{r}} - \delta t_n^{\mathrm{SV}}] + I_n + T_n + \varepsilon_n$$

This pseudorange computation formula is also the one used in this thesis.

2.1.2 Main Error Factors for Positioning

As mentioned above, GPS uses pseudorange in positioning and signal propagation time to compute the pseudorange. In these procedures, there are several places where errors

could be introduced. Usually the errors can be either random or has some kind of pattern. Also the cause for the errors can be directly from satellites, from propagation path or from the receiver. The following part of this section will focus on some main errors and solutions for most of the errors.

Firstly, the errors caused by the satellites are satellite clock bias and satellite coordinate bias. The GPS satellites use atomic timepieces to record time. Accurate as the timepieces are, they can have some bias. The ephemeris information sent by the satellites contain the clock correction $a_{f_0}, a_{f_1}, a_{f_2}$ that can be used to compute the accurate time based on GPS time. The equation is as follow:

$$\delta t^{sv} = a_{f_0} + a_{f_1}(t - t_{oc}) + a_{f_2}(t - t_{oc})^2 + \Delta t_r$$

This bias can sometimes cause positioning error around 5m [5]. And with the development of science, satellites with new atomic timepieces have been launched so that error caused by satellite clock bias is being minimized.

Secondly, while penetrating the earth atmosphere, the signal has to go through ionosphere and troposphere,as Fig. 2.4 illustrates, which will slow down the propagation speed because sun activity and geomagnetic activity.

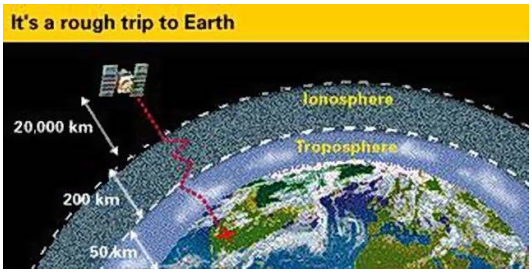

図 2.4: GPS signal must go through ionosphere and troposphere to reach the planet surface

Because the ionospheric and tropospheric errors can be effected by temperature, humidity, seasons and day night alternation, it is very difficult to predict the exact time delay for the ionospheric and tropospheric errors. Fortunately, accurate models have been developed to calculate both ionospheric and tropospheric delays. Klobuchar model for ionospheric delay and Saastamoinen model for tropospheric delay.

In Klobuchar model, the ionospheric delay I can be computed with the following equation:

$$\frac{I}{c} = \begin{array}{ll} A_1 + A_2 \cos\left(\dfrac{2\pi(t - A_3)}{A_4}\right), & \text{if} |t - A_3| < A_4/4 \\ A_1, & \text{otherwise} \end{array}$$

where A_1 is the delay in the night $(5 \times 10^{-9} s)$, A_2 is the amplitude of cosin function

used in day time A_3 is the phase of the cosin function and A_4 is the period of the cosin function. Although Klobuchar can not perfectly solve the ionospheric delay, it can correct 50% of the error caused by ionosphere. [6]

Different to the ionospheric delay which is caused by ionization, tropospheric delay is caused mainly by the dry air water vapor that refracts signal. To solve this problem, Saastamoinen model [7, 8] is proposed.

$$T = \frac{2.277 \cdot 10^{-3}}{\cos z} \left[P + \left(\frac{1255}{T} + 0.05 \right) e - B \tan^2 z \right] + \delta R$$

In this equation, z is the elevation angle of the satellite, T is temperature, P is barometric pressure, e is water vapor partial pressure, B is a correction factor to the height, and δR is the correction term.

Thirdly, the receiver's noise can also cause considerable error. The receiver's noise is caused by antenna, cable, shaking and environmental factors. These errors can not be modeled and are hard to digitalized. And usually, these kinds of error do not effect the positioning result very much.

In conclusion, there are mainly three kinds of categories for GPS positioning errors. Each category of error is caused by different factors and their influence on the positioning result varies. The following table shows these errors, their causes and their effect on positioning result.

Source of Error	Cause	Properties of Error
Satellites	Orbit factors	2 m (bias)
	Clock offset	2 m (bias))
Signal propagation	Ionospheric delay	2 ∼around 10 m (bias)
	Tropospheric delay	2.3 ∼ 2.6 m (bias)
	Multipath	∼ 100 m (random)
Receiver based	pseudorange calculation noise	∼ 1 m(random)

2.2 Related Works

In order to obtain higher accuracy of GPS positioning results in urban canyon environments, several approaches have been discussed. One of ideas is to sensor fusion. GPS alone is not sufficient in urban area, so combining all kinds of sensor together to get higher accuracy seems reasonable. For instance, the combination with LiDAR [9], Laser [10] and 3D Laser Scanner [11]. Besides the sensor fusion method, researches focus on multipath mitigation have also been done. The multipath effect could be mitigated based on different approaches, and mainly cataloged by three: antenna-based [12], receiver-based [13], and navigation-processor-based [14] techniques. Multipath mitigation using correlator

has also been researched recently. Most of the commercial level GPS receiver is equipped with narrow correlator to deal with small multipath. Usually there are two ways of correct multipath effect. The first one is to digitalize the multipath error, and use this number to correct pseudorange [15]. The second method is to use a sophisticated algorithm to recognize the clear signals (signals that are not effected by multipath) and only use the clean signals in the positioning procedure [16]. In additin, a method called RAIM (Receiver Autonomous Integrity Monitoring) was proposed by [17, 18] to select the reliable signals in the least square procedure. But this method is difficult to apply in an urban environment where more than half of the signals are effected by multipath [19]. Besides, since the single strength is greatly effected by the elevation angle of the satellite, an idea of recognizing LOS signal based on the elevation angle is proposed [20]. However, GPS signal strength is based on not only elevation angle but also on the properties of antenna and cable. Also, in urban area where multipath frequently happens, the signal strength can vary a lot. As a result, new methods should be researched to deal with the urban environment.

Besides using only GPS data, ideas that combine other data with GPS data to improve the positioning accuracy have also been proposed. For instance, Obst [21] and Miura [2] proposed ray tracing algorithm using 3D map of urban area, as illustrated by Fig. 2.5 and Fig. 2.6, to detect whether a signal is blocked by building. As can be observed, the 3D building geometry of the urban area is created based on reliable 2D and building height data. After creating the 3D map, ray tracing can be performed so that LOS, NLOS and multipath signals can be detected.

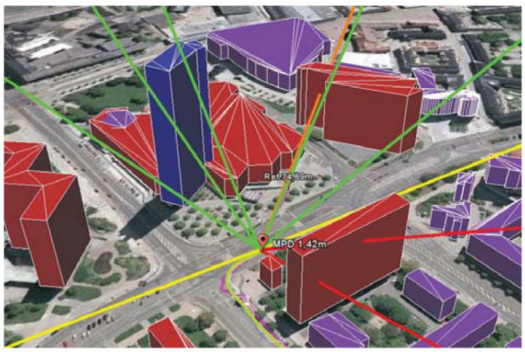

図 2.5: Ray tracing result of Obst

Since this thesis is based on the ray tracing method proposed by Miura, Miura's ray tracing method will be introduced in this chapter.

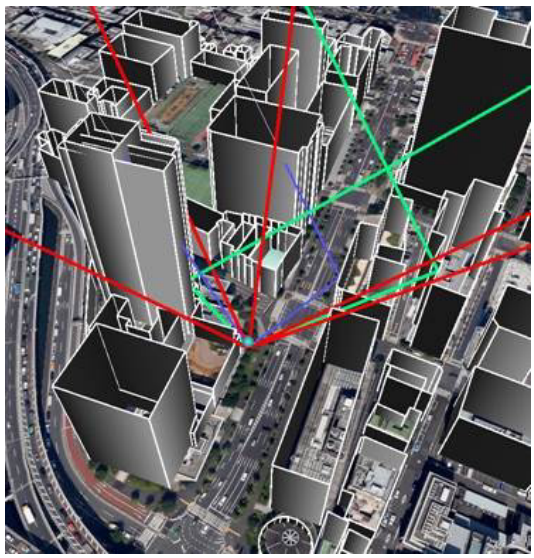

図 2.6: Ray tracing result of Miura

2.2.1 3D Map and Ray tracing

In this section, the 3D map and ray tracing algorithm that are used in Miura's paper will be introduced. Since this thesis is based on Miura's research, the 3D map and ray tracing algorithm is also used in the results in this thesis.

Firstly, the composition of 3D map. The 3D map used in this research is composed of 2 sets of data. The first one is building peripheral line data, as denoted in (a) of Fig. 2.8, which can be downloaded from the Geospatial Information Authority of Japan website for free. And the data displayed in the figure is the data of Hitotsubashi area of Tokyo.

The second set of data is the point cloud data. As (b) of Fig. 2.8 denotes, the points cloud data is written in a text file with one line represents on point (longitude, latitude, height). This data set can be bought from a Japanese company called Asahi. There is one problem of this data set, which is the time of measurement. The data used in this research is measured in 2008, which is nearly 7 years ago. Luckily, the building geometry hasn't changed a lot in the Hitotsubashi area, which is the main experiment area of this thesis.

After acquiring these 2 sets of data, the composition of the 3D map can begin. Based on the corner points displayed in the 2D building peripheral data, which is a corner of a building, a height is searched through the point cloud data to find the nearest (longitude, latitude, height) point to the corner and set that height to the point in 2D data. Usually a building can have several corner points in the 2D data and in this thesis, all these corner points of a same building are set to the same height. Fig. **??** denotes the 3D map used in

8	139.753318	35.688306	4.91
9	139.753329	35.688306	4.71
10	139.753341	35.688306	4.70
11	139.753352	35.688306	4.72
12	139.753363	35.688306	4.72
13	139.753374	35.688306	4.71
14	139.753385	35.688306	4.70
15	139.753396	35.688306	4.72
16	139.753407	35.688306	4.91
17	139.753418	35.688306	4.73
18	139.753429	35.688306	4.74
19	139.753440	35.688306	4.73
20	139.753451	35.688306	4.72
21	139.753462	35.688306	4.71

(a) The building peripheral line used in 3D map composition

(b) Point cloud data for building height used in 3D map composition

図 2.7: 2D building peripheral line and point cloud data used in 3D map composition

the thesis an the software used to display is Google Earth. As can be observed, there are no roofs to any of those buildings displayed. The reason is that roof is not needed when trying to detect a NLOS satellite or a reflected path. Adding roofs to the 3D map will only increase the computation load.

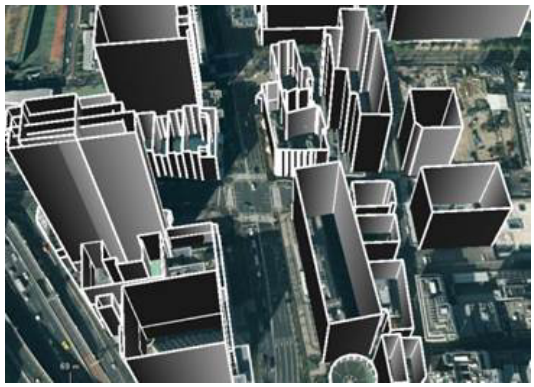

図 2.8: The 3D map used in this thesis and displayed on Google earth software

Secondly, the ray tracing algorithm. Ray tracing, as in Fig. 2.9, is firstly invented in computer graphic to simulate the propagation of light.

But recently, this method has also been used in the simulation of electronic wave propagation [22, 23] since the signal propagates similar to that of light. And similarly, the fundamental of ray tracing algorithm is displayed in Fig. 2.10.

As shown in Fig. 2.10, if the plane is considered as a mirror surface and can reflect the light (signals) bases on the law of physics. And a satellite is considered as a source of light (signal), the image of people in the figure is the receiving end of the signal. Following all the assumptions above, the people's mirror positioning (illustrated as dashed line human figure) to the plane is firstly computed based on the position of the solid line human figure

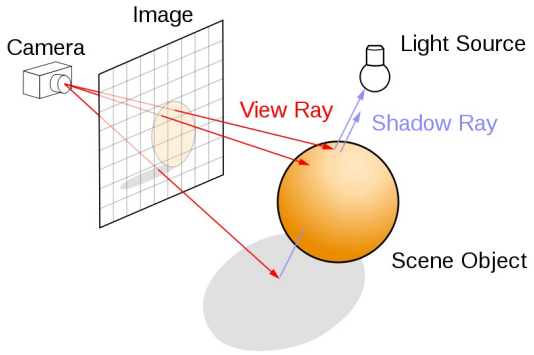

図 2.9: Ray tracing method used in computer graphics to simulate the propagation of light

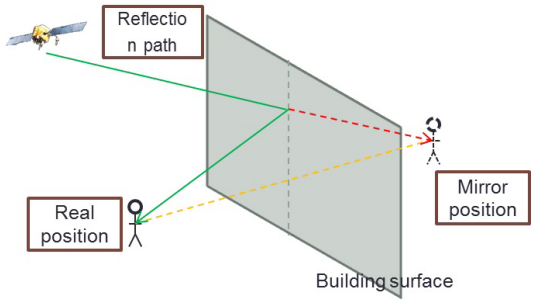

図 2.10: The illustration of the ray tracing algorithm of detecting reflected path

and the position of the plane. After step one, a line is drawn connecting the satellite and the dashed line human figure. If the line has a crossing point with the plane then it is clear that there is a possible reflection path from the satellite to the solid line human figure (display as a green curved line). After detecting the green line, the first segment, the one that connects satellite and crossing point, and the second segment, the one that connects the crossing point and the solid line human figure, can be acquired. And if there are no other planes that cut off these two segments, then we say that the green line detected is valid. This green line is called a reflected path and is assumed as what really happened when the data is collected.

Similarly, the ray tracing algorithm can be used in the detection of NLOS satellites. As shown in Fig. 2.11, when trying to decide whether a satellite is a NLOS satellite, we simply draw a line connecting the satellite and the solid human figure. And if this line is cut off by any of the planes in our 3D map, then it is clear that this satellite is not visible from the position of the solid human figure, which means this satellite is not a LOS but a NLOS satellite.

The detailed algorithm of detecting reflection path and NLOS is listed in Algorithm 1 and Algorithm 2.

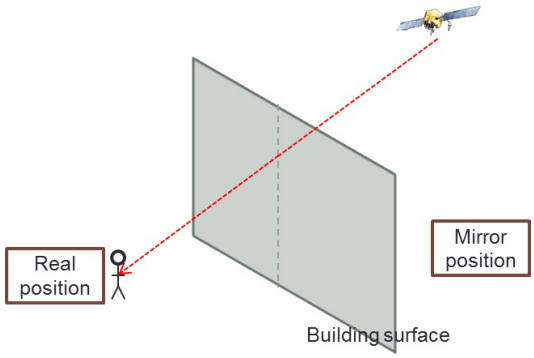

図 2.11: The illustration of the ray tracing algorithm of detecting NLOS satellites

Algorithm 1 The detection of reflected path satellites

1: Calculate a mirror position (dashed line human figure) of a fixed ground point (solid line human figure) to a known plane.
2: Connect the satellite and the mirror position.
3: Detect the crossing point of the line and the plane.
4: **if** The crossing point exists **then**
5: Connect the satellite and the crossing point, the crossing point and the fixed ground position.
6: **if** Either of the two line segments is cut off **then**
7: The reflection path doesn't exist.
8: **else**
9: A reflection path is found.
10: **end if**
11: **else**
12: The reflection path doesn't exist.
13: **end if**

2.2.2　GPS Positioning with 3D Map and Ray Tracing Algorithm

As stated in the section above, researches have already been done to combine GPS positioning method and the 3D map and ray tracing algorithm. In this chapter, this method will be introduced in detail.

Fig. 2.12 shows the flow chart of Miura's 3D map and ray tracing method. In his research, the GPS data is acquired from a receiver called ublox-6, which is a receiver for GPS-only purpose. Meanwhile, his method is an offline method, which means all data are processed afterward. In the flowchart, the step "Estimated user positions and measurements by commercial GPS receiver" is done by the ublox-6 receiver and this

Algorithm 2 The detection of NLOS satellites

1: Connect the satellite and the fixed ground point (solid line human figure).
2: Exam all the planes in the 3D map and the line.
3: **if** The crossing point exists **then**
4: The signal from this satellite is NLOS.
5: The satellite is a NLOS satellite.
6: **else**
7: The signal from this satellite can reach the receiver.
8: The satellite is a LOS satellite.
9: **end if**

receiver-output position will be used in the following steps. The "SV positions" means space satellite positions, namely satellite positions, and the positions are calculated based on the "Ephemeris" information output by the receiver. The calculation part has already been summarized into libraries and therefore no introduction will be given here. The "developed 3D MAP(2D+DSM)" is the 3D map introduced in the sections above. Ionospheric and tropospheric and broadcast ephemeris delay models, which are also introduced in the sections above, are also summarized in libraries so no further introductions will be given here. Besides a receiver calculated position, ublox-6 can also give some raw measurement data, including the signal strength and measured pseudorange, which are key data in the research and will be introduced below.

Fig. 2.13 shows the detailed figures of several important steps in the method. In Fig. 2.13a, the step of "Generating samples based on the receiver estimated position and system prediction" is displayed. As can be observed, the two yellow pins represent the receiver estimated position and the system prediction position. The system prediction position means the result of the method of the last epoch of GPS time. The green dots around the two yellow pins are sample points generated randomly based on Gauss function. These sample points are assumed to be the receiver's real position when the data is gathered. The number of the sample points are 200 with 100 around the receiver estimated position and the other 100 around the system prediction position. Since the number of the sample points can effect the processing time greatly, 200 is reasonable in this situation.

After distributing the sample points, the ray tracing algorithm is applied to every sample points, as denoted in Fig. 2.13b. In the figure, the white line denotes NLOS satellite, the red line is signal from LOS satellites and the green line represents a reflection path found by the ray tracing, which is a reflection path from a NLOS satellite in this case. To distance error caused by the reflection path, represented as $\varepsilon^{\text{reflection}}$, the following equation is used:

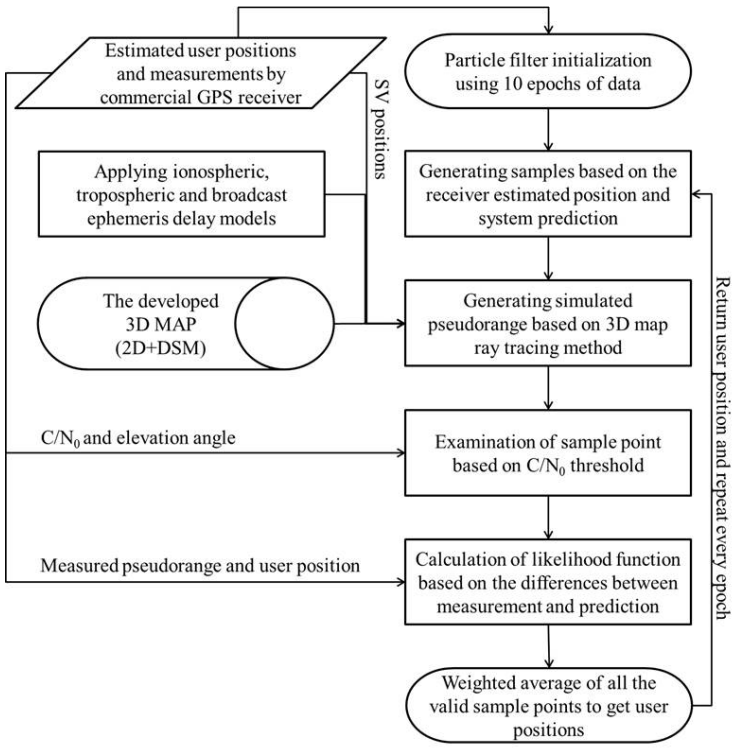

図 2.12: The flow chart of Miura's GPS positioning with 3D map and ray tracing algorithm method

$$\varepsilon^{\text{reflection}} = \|x_n - x^{\text{reflection}}\| + \|x - x^{\text{reflection}}\| - \|x_n - x\|$$

where x represents the coordinate of the satellite, x_n is the coordinate of the sample point n and $x^{reflection}$ is the reflection point located on the surface of the plane.

After computing the $\varepsilon^{\text{reflection}}$, a simulated pseudorange will be computed. The equation is list at the following:

$$simR_n = \rho_n + c(\delta t^{\text{r}} - \delta T_n) + I_n + T_n + \varepsilon^{multipath}$$

where $simR_n$ represents the simulated pseudorange of satellite n, ρ_n denotes the geometric distance between the satellite and the sample point, δt^{r} and δT_n represent the clock offset of the receiver and the clock offset of the satellite, I_n and T_n are ionospheric delay and tropospheric delay, which are calculated using the Klobuchar and Saastamoinen models introduced above, and $\varepsilon^{multipath}$ represents the distance error caused by reflection, which is the result of the ray tracing process. This simulated pseudorange is the a simulation of what really happened when the data was gathered and if the sample point is near the ground truth, the this simulated pseudorange is suppose to be similar to the measured pseudorange output by the receiver.

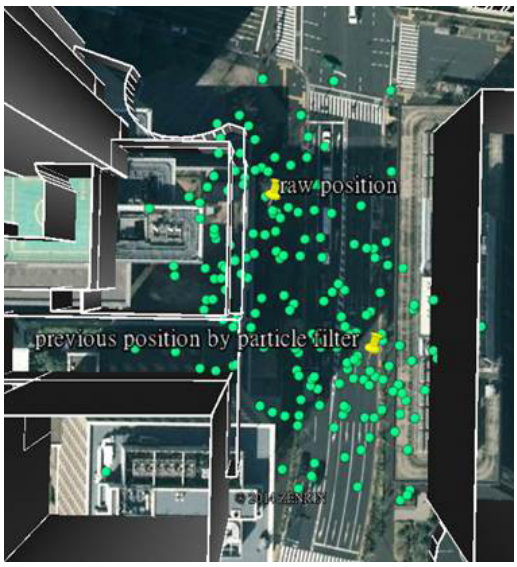

(a) Distribution of sample points based on 2 center positions

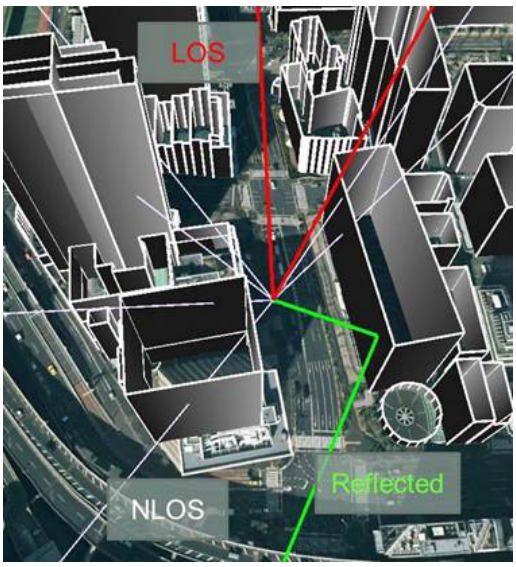

(b) Apply ray tracing to every sample points generated in (a)

(c) Calculate the weight factor of every sample points

(d) Calculate the average of all sample points

図 2.13: Figures illustrate every important steps in the 3D map with ray tracing method

Fig. 2.13c show the result of similarity judgement using the measured pseudorange and the simulated pseudorange. After acquiring the simulated pseudorange in (b), two types of similarity are examed. The first one is the similarity between the measured pseudorange and the simulated pseudorange. For instance, if the number of signals received at this GPS time epoch, then the measured pseudorange is $\boldsymbol{meaR} = [meaR_1, meaR, \cdots_2, meaR_N]^T$ and the simulated pseudorange from the n satellites is presented as $\boldsymbol{simR} = [simR_1, simR_2, \cdots, simR_{N^{sim}}]^T$. After acquiring

these two sets of pseudorange from receiver and ray tracing, the similarity of these two sets can be calculated. The equation for this is:

$$diff^{pr(i)} = \min_{\delta t^{r(i)}} \sum_{n}^{N^{sim}} \frac{|\boldsymbol{meaR_n} - \boldsymbol{simR_n}|}{N^{sim}}$$

where $diff^{pr(i)}$ denotes the similarity of the two sets of pseudorange, $\boldsymbol{meaR_n}$ and $\boldsymbol{simR_n}$ are measured pseudorange and simulated pseudorange and N^{sim} is the number of valid satellites that ray traced. Because the receiver clock bias $\delta t^{r(i)}$ is difficult to calculate and is the same to all the ray traced satellites, in this equation we tries to find the appropriate $\delta t^{r(i)}$ to minimize $diff^{pr(i)}$, and set this minimized similarity as this sample point's pseudorange similarity.

In addition to pseudorange similarity, another similarity, positioning similarity is also a criterion to decided whether the sample point is valid or not. Alike to the pseudorange similarity, there are also two positions are calculated to every GPS time epoch. The first position is calculated using the measure pseudorange set and the second position is calculated using the simulated pseudorange from a sample point. As a result, the first position only need to be computed once for every GPS time epoch and the second position should be calculated as many times as the number of sample points. In Fig. 2.13c, the blue bubbles displayed are the second positions computed based on the simulated pseudorange sets of the green sample points. After acquiring these two positions, the similarity of these two positions is calculated for each sample points. The equation for this similarity is :

$$diff^{pos(i)} = \|\boldsymbol{y}^{(i)} - \boldsymbol{y}_{GPS}\|$$

where $diff^{pos(i)}$ illustrates the similarity of the sample point, $\boldsymbol{y}_{GPS}$ is the coordinates of the position computed using the measured pseudorange, $\boldsymbol{y}^{(i)}$ represents the coordinates of the position computed using the simulated pseudorange. This similarity is simply the geometric distance between these two distance.

Fig. 2.13c presents how every sample points are evaluated. The validity of a sample point is judged firstly. When a sample point satisfies the following three terms, we say that this sample point is valid.

- This sample point must be outside of all buildings recorded in the 3D map.
- If the signal strength of satellite N is strong (only a LOS signal could have such signal strength) and the ray tracing result from this sample point proves that the satellite is LOS.
- If the signal strength of satellite N is weak (only a NLOS satellite whose signal reaches the receiver through reflection) and the ray tracing result from this sample point proves that the satellite is NLOS.

After the validity check for all the sample points, a weight is calculated for every valid sample point remaining. And the criteria of the weight calculating are the two similarity values, pseudorange similarity and positioning similarity, acquired from the former steps. The equation for the weight computation is :

$$\alpha^{(i)}(t) = L^{(i)}_{pseudorange} L^{(i)}_{positioning}$$

where $\alpha^{(i)}(t)$ represents the weight of a sample point, $L^{(i)}_{pseudorange}$ and $L^{(i)}_{positioning}$ are factors computed based on the $diff^{pr(i)}$ and $diff^{pos(i)}$ computed from the equations above.

The equations for $L^{(i)}_{pseudorange}$ and $L^{(i)}_{positioning}$ are:

$$L^{(i)}_{pseudorange} = \begin{cases} \exp\left[-\left(\dfrac{diff^{pr(i)}}{\sigma_{pr}}\right)^2\right] & (diff^{pr(i)} < C_1) \\ 0 & (otherwise) \end{cases}$$

$$L^{(i)}_{positioning} = \begin{cases} \exp\left[-\left(\dfrac{diff^{pos(i)}}{\sigma_{GPS}}\right)^2\right] & (diff^{pos(i)} < C_2) \\ 0 & (otherwise) \end{cases}$$

where $L^{(i)}_{pseudorange}$ and $L^{(i)}_{positioning}$ are two factors for weight based on the pseudorange and positioning similarity, $diff^{pr(i)}$ and $diff^{pos(i)}$ are the pseudorange and positioning similarities calculated by the equations above. C_1 and C_2 are two empirical constants, which are set to 8 and 40 in Miura's research. σ_{pr} and σ_{GPS} are also constants.

After weighting every valid sample points remaining, as illustrated as the cyan dots in Fig. 2.13d, the weighted average is calculated, the equation is listed as follow.

$$\boldsymbol{x}(t) = \frac{\sum_i \alpha^{(i)}(t) \boldsymbol{P}^{(i)}(t)}{\sum_i \alpha^{(i)}(t)}$$

where $\boldsymbol{x}(t)$ represents the final result, as illustrated by the big yellow dot in Fig. 2.13d, $\alpha^{(i)}(t)$ means the weight of sample point i at GPS time epoch t and $\boldsymbol{P}^{(i)}(t)$ is the coordinates of sample point i at GPS time epoch t.

In conclusion, at every GPS time epoch when a result is output by the receiver, sample points are generated by a Gauss function around the receiver-output point and the result output by the 3D map and ray tracing algorithm of last GPS time epoch. To every sample point ray tracing algorithm is applied and a set of simulated pseudorange from every satellite is computed. Based on this simulated pseudorange and the measured pseudorange output by the receiver, two similarity values are calculated. The first similarity value is called the pseudorange similarity, which is the similarity between the simulated pseudorange set and the measured pseudorange set. The second similarity value is the

positioning similarity, which is the geometric distance between the one position calculated by the measured pseudorange and the other position calculated using the simulated pseudorange. After the similarity evaluation is applied to all the sample points, the weight average of all sample points is calculated. And this weight average is the final result of the 3D map with ray tracing method, which is in turn used as a center of the sample points at the next GPS time epoch.

第 3 章

Using multi-GNSS in 3D Map with Ray Tracing Method

As introduced above, Miura's 3D map with ray tracing method only uses GPS, and multi-GNSS is being developed rapidly throughout the world. As a result combining another GNSS in the method to increase the overall usable satellites in the earth orbit seems to be a perfect way to increase the accuracy of the positioning. In this chapter a brief introduction of Russia GLONASS, the common method of multi-GNSS positioning and the algorithm of combining GLONASS and GPS in the 3D map with ray tracing method will be introduced.

3.1 Multi-GNSS Method Overview

Positioning problem has been a headache for the world for a long time. Since the America GPS achieves its success, countries around the world have been trying to replica this success by developing their own navigation satellite systems and launching their own satellites into the earth orbit. Besides the existing GPS and GLONASS, some other countries' navigation projects have been proved to be very promising, for instance, the China BeiDou global navigation system, European GALILEO global navigation system, and Japan QZSS regional navigation system.

Many research has been done to investigate the benefit of multi-GNSS. For example, [**?**] has simulated the number of usable satellites in 2020 when GALILEO and BeiDou (compass) are fully developed. In 2020, among all the usable satellites in the orbit, GPS satellites, which is the main navigation system available currently, will only be 27%, GLONASS alike will be only 20%, the rest, which is Galelio plus compass, will occupies 53% of all usbal satellites. And for all scenarios, vehicle or pedestrian, junctions or not, the number of usable satellites will always be more than 12, which means that the era of insufficiency of usable satellites in urban area will end.

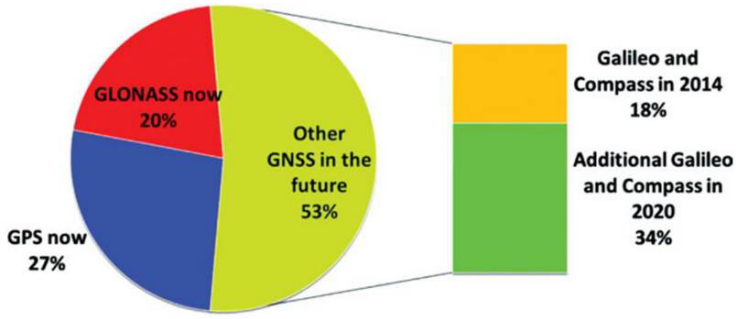

(a) The percentage of satellites from different navigation systems in 2014 and 2020

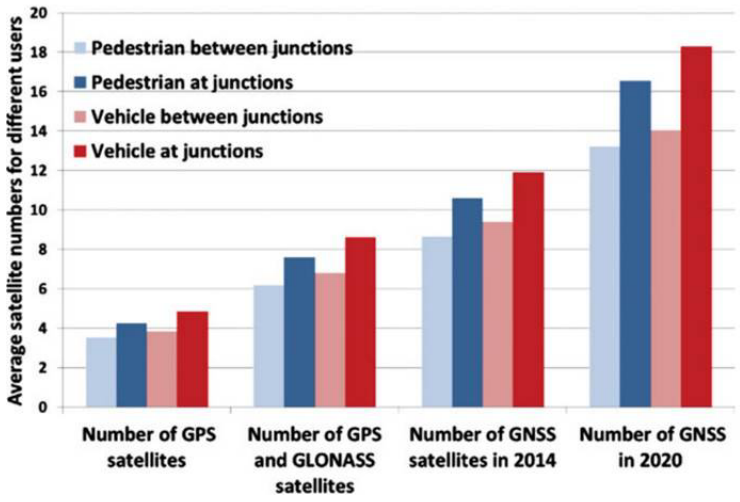

(b) Usable GNSS satellites from different navigation systems for different scenarios

図 3.1: The current situation and the future development of the number of usable multi-GNSS satellites

Therefore, using multi-GNSS is very wise when one tries to improve the available satellite in urban area. Since GLONASS is the only developed navigation system beside GPS currently, we will choose to add GLONASS into the system and the following is a brief introduction of GLONASS.

GLONASS (GLObal'naya NAvigatsionnaya Sputnikovaya Sistema), like America GPS, is a space-based satellite navigation system operated by the Russian Aerospace Defence Forces. It provides an alternative to Global Positioning System (GPS) and is the second alternative navigational system in operation with global coverage and of comparable precision. The GLONASS project began in the Soviet Union in 1976, and in October 2011, the full orbital constellation of 24 satellites was restored, enabling full global coverage.

Fig. 3.2 displays the orbit height of GPS, GLONASS, Galileo and Compass. GLONASS

provides real time position and velocity determination for military and civilian users. The satellites are located in middle circular orbit at 19,100 km altitude with a 64.8 degree inclination and a period of 11 hours and 15 minutes.[24, 25]

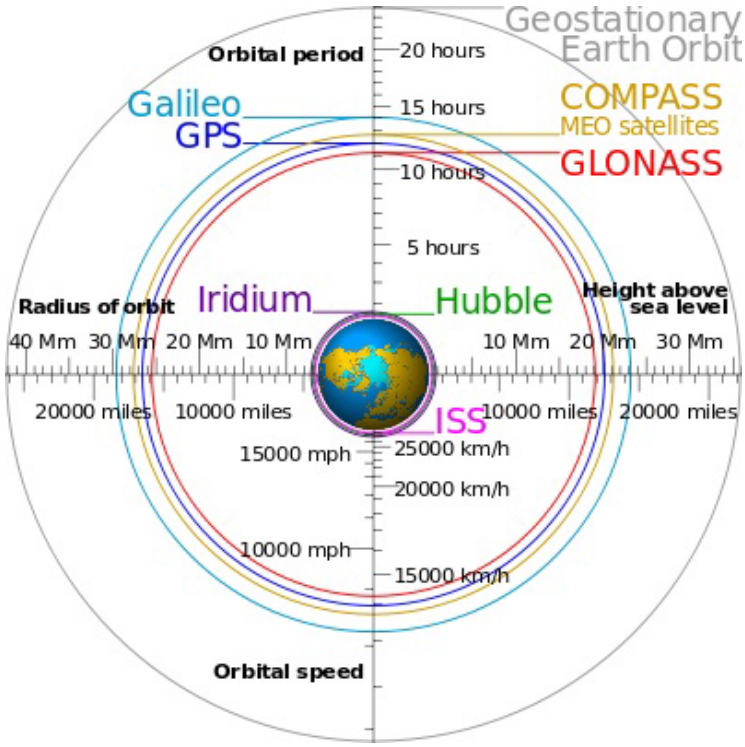

図 3.2: The orbit height of GPS, GLONASS, Galileo and Compass

GLONASS satellites, similar to GPS, transmit two types of signal: open standard-precision signal L1OF/L2OF, and obfuscated high-precision signal L1SF/L2SF. In this thesis, the open standard-precision signal is used. The following table displays some properties of GLONASS and GPS. [26]

name	GPS	GLONASS
The basic principle of measurement	code	code
State	USA	Russia
Launch of satellites	1978	1982
Number of satellites	32	24
Inclination[degree]	55	65
Number of orbit	6	5
Altutude orbit[km]	20200MEO	19100MEO
Circulation time[hh:mm]	11:58	11:15

In conclusion, the global coverage 24 satellites GLONASS, except GPS, is the most

mature GNSS existing in the world.

3.2 Combination of GLONASS and GPS

As introduced above, there are GALILEO, Beidou, QZSS and many other GNSS in the world, why choose GLONASS to combine with GPS? There are several reasons for choosing GLONASS in the multi-GNSS in this these.

- GLONASS is a mature GNSS and has 24 satellites in orbit, whereas other GNSSs is being developed and don't have such many available satellites.
- On the receiver part, many multi-GNSS receiver manufacturers have products that can receiver both GLONASS and GPS signals. The receiver designed for the combination of GPS with other GNSS signals is rare.

Fig. 3.3 shows the research done by [26] concerning the multi-GNSS of GLONASS and GPS. As can be observed from the figure, for the terminal users, especially in the high latitude areas, the accuracy of using GPS+GLONASS is +15% to + 30% better than GPS alone. And the usable satellites number increases from 8-12 of GPS alone to 14-20 of GLP+GLONASS.

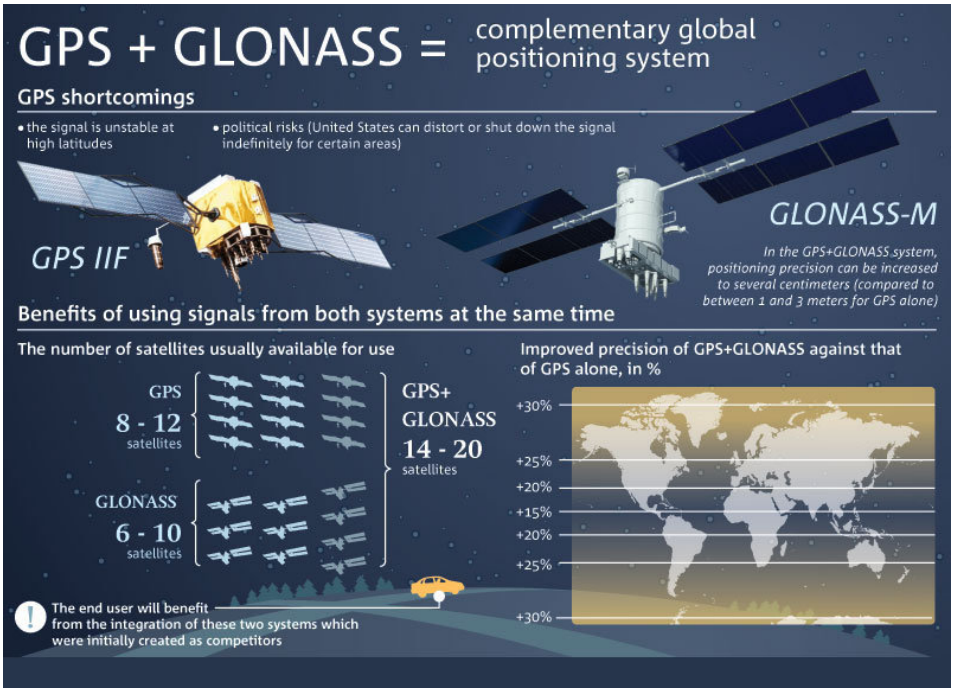

図 3.3: The benefit of combining GPS and GLONSS

In conclusion, as the most developed two GNSSs in the world, the combination of GLONASS and GPS will undoubtly increase the number of usable satellites and position-

ing accuracy. Therefore, in this thesis, a method that adding GLONASS into the 3D map with ray tracing method is proposed and realized. The following sections will introduce the methodology and the results.

3.2.1 The Weighted Least Square for multi-GNSS

In GPS alone scenario, the weighted least square equations are fairly simple, which are displayed by the following equation.

$$R = \begin{bmatrix} R_1 \\ R_2 \\ \vdots \\ R_N \end{bmatrix} = \begin{bmatrix} \parallel x_1^{SV} - x^r \parallel + c\delta t^r \\ \parallel x_2^{SV} - x^r \parallel + c\delta t^r \\ \vdots \\ \parallel x_N^{SV} - x^r \parallel + c\delta t^r \end{bmatrix}$$

where $R_1 R_2 \dots R_N$ are measured pseudorange of N satellites, x_1^{SV} is the ECEF (earth-centered-earth-fixed) coordinates of receiver and δt^r is the receiver clock bias. In this case, a position can be computed as long as N is larger than 4.

When combined with GLONASS satellites, however, the weighted least square equations changes. Besides, the time recording are different between these two systems. The formula used to synchronize the two time systems are listed as follow.

$$t_{glo} = t_{gps} + 3hours - leapseconds$$

The equation for the multi-GNSS is listed as follow.

$$\begin{bmatrix} R^{gps1} - \rho^{gps1} \\ \vdots \\ R^{gpsN} - \rho^{gpsN} \\ R^{glo1} - \rho^{glo1} \\ \vdots \\ R^{gloN} - \rho^{gloN} \end{bmatrix} = \begin{bmatrix} a_x^{gps1} & a_y^{gps1} & a_z^{gps1} & 1 & 0 \\ \vdots & \vdots & \vdots & \vdots & \vdots \\ a_x^{gpsN} & a_y^{gpsN} & a_z^{gpsN} & 1 & 0 \\ a_x^{glo1} & a_y^{glo1} & a_z^{glo1} & 0 & 1 \\ \vdots & \vdots & \vdots & \vdots & \vdots \\ a_x^{gloN} & a_y^{gloN} & a_z^{gloN} & 0 & 1 \end{bmatrix} \begin{bmatrix} \delta p_x \\ \delta p_y \\ \delta p_z \\ \delta t_{gps} \\ \delta t_{glo} \end{bmatrix}$$

In this equation, δp_x, δp_y and δp_z are receiver's ECEF position, which are unknown and needed to be calculated, δt_{gps} and δt_{glo} are receiver's clock bias to GPS system and GLONASS system respectively, since the two GNSSs have their own time recording systems, which is introduced above, these two are different and needed to be calculated. $(a_x^{gpsN}, a_y^{gpsN}, a_z^{gpsN})$ and $(a_x^{gloN}, a_y^{gloN}, a_z^{gloN})$ are the satellites coordinates of GPS and GLONASS respectively. On the left side of the equation, R^{gps} and R^{glo} are the geometric distance between the satellites and a receiver and ρ^{gps} and ρ^{glo} are the measured pseudorange output by the receiver.

3.2.2 The 3D Map with Ray Tracing for GPS and GLONASS

Besides the weight least square part, the similarity calculation part between GPS alone and GPS plus GLONASS are different.

In GPS alone scenario, which is already introduced above, uses only GPS signal, which has only one receiver's clock bias toward the GPS. In GPS plus GLONASS scenario, however, receiver's clock bias increases into two, one toward GPS and the other one toward GLONASS. Hence, the similarity calculation part should be modified accordingly.

There are 32 satellites in the GPS system and 24 satellites in GLONASS system. As a result 56 satellite signals can possiblely be received by the receiver. In the 3D map and ray tracing algorithm, every satellite has a number (PRN) which is different from other satellites. Here the 1 to 32 GPS satellites are assigned as PRN 1 to 32 and 1 to 24 GLONASS satellites are assigned as 33 to 56. By judging the PRN number of the signal, we can understand which GNSS system does the signal came from and apply the different similarity calculation algorithm.

Here, the receiver clock bias to GPS is set as the reference, which means 0. And the receiver clock bias to GLONASS is calculated based on the GPS clock bias. The following two equations illustrates the receiver clock biases for both GPS and GLONASS.

$$biasGPS = 0$$

$$biasGLO = (\delta t_{glo} - \delta t_{gps}) * c$$

where $biasGPS$ means the receiver clock bias for GPS and $biasGLO$ means the receiver clock bias for GLONASS, and δt_{glo} and δt_{gps} are clock biases calculated in the weighted least square method mentioned above and c is the speed of light. The reason for setting the $biasGPS$ to 0 is because the robustness of the program.

After getting these two factors, the length of reflection path can be calculated. In NLOS case, if any reflection path can be found from a specific satellite to a specific sample point, the simulated pseudorange will be assigned as the length of the reflected path, and the similarity between the measured pseudorange and the simulated pseudorange are calculated using the following equations.

To GPS:

$$similarity_{GPS} = simR - meaR + biasGPS - optimum$$

And to GLONASS:

$$similarity_{GLO} = simR - meaR + biasGLO - optimum$$

where $similarity$ is the similarity result, $simR$ and $meaR$ mean simulated pseudorange and measured pseudorange respectively and $optimum$ is a compensation number that

図 3.4: The geometric layout of the experiment area of Hitotsubashi, Tokyo

remain the same for all the satellites of this sample point and make the summary of this similarity of all satellites of this sample point reaches its minimum.

As to the position similarity in GPS plus GLONASS method, it remains the same. The only part that changed is the weighted least square used to calculate the position, which is also introduced above.

3.3 Experiment and Results

3.3.1 Experiment Setup

To prove the efficiency of adding GLONASS to the current GPS with 3D map and ray tracing method, experiments have been conducted at one of the urban canyon area in Hitotsubashi, Tokyo. Fig. 3.5 shows the geometric layout of the experiment area, and the cyan line illustrates the ground truth of the dynamic experiment and the red T bubble illustrates the location for the static experiment.

In this experiment, the data is collected in two cases, the normal case and the difficult case. The definition of normal and difficult is based on the number of usable satellites. Fig. **??** shows the details of the experiment. The experiment is conducted at April 18th, 2014. The y-axis, number of visible SV, denotes the GPS satellites with elevation angle above 10 degree and the x-axis denotes the time of the day. Since GPS has more available satellites than GLONASS and when used separately, the positioning accuracy of GPS alone is better than that of GLONASS alone, the main system in this thesis is GPS and

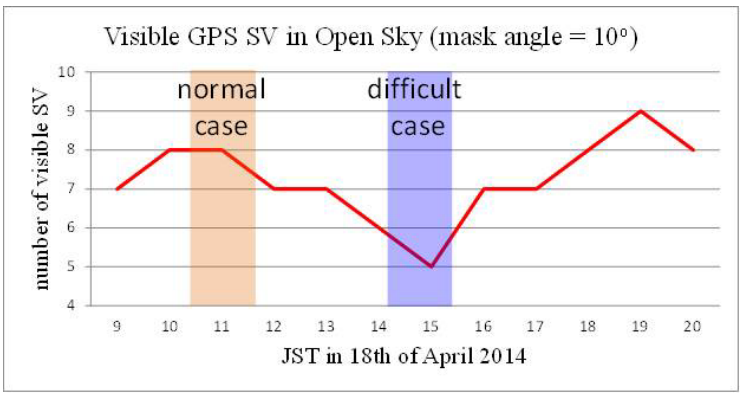

図 3.5: Satellite number and experiment time for normal and difficult cases

表 3.1: Definition of the scenarios and data collection date

Scenario	GPS SV in open field	Data of collection
Good	more than 8	18th of June
Normal	7 to 8	24th of April and 14th of July
Difficult	5 to 6	18th of April and 25th of July

the definition of normal and difficult is based on the visible satellites from GPS. The normal case data is collected from 10:30 to 11:30, when satellite number is around 8 and difficult case data is collected from 14:00 to 15:00, when the satellite number is 5 or 6.

The the following table contains the explanation of scenarios and the data when the data used is collected.

Fig. 3.6 shows the receiver used in this research. This device is u-blox EVK-M8C commercial level receiver and it can collect both GPS and GLONASS data. Also it can output ray measurement data, which is the measured pseudorange introduced above.

3.3.2 Results and Analysis

In this section, the result of the experiments and analysis will be displayed. In the experiment, the dynamic and static experiments are conducted and the result figures will be shown according to GPS and GPS plus GLONASS. Because the u-blox8 receiver uses some kind of filter, which is obvious if one observes the result output, to smooth its result and we have no way of knowing what happened inside the receiver, another result, GPS single point positioning and GPS+GLONASS single point positioning, is displayed. This result is calculated merely by putting data into the weighted least square. The software used for the display is Google Earth.

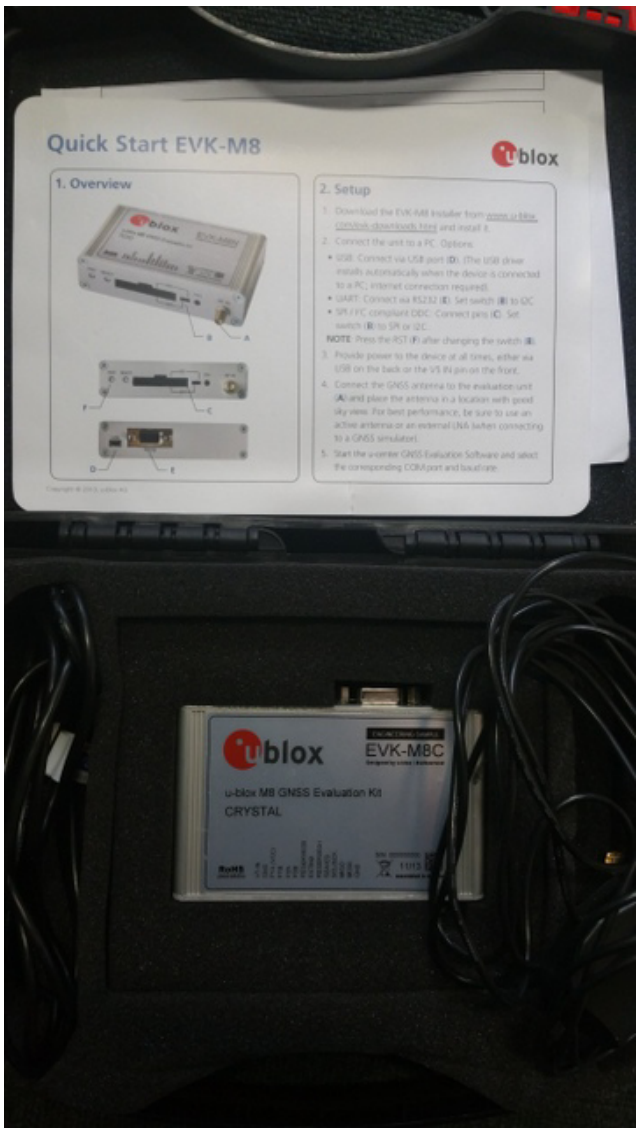

図 3.6: U-blox receiver used to collect GPS and GLONASS data

Fig. 3.7 contains the results of GPS and GPS plus GLONASS. The upper figure shows the result of u-blox8 output (red rectangular), GPS with 3D map and ray tracing method (yellow dots), GPS single point positioning (pink triangle) and ground truth (cyan line).

As can be observed from the result figure, for GPS's normal and difficult cases, the receiver can always give smooth result trajectory. At the intersection, where signals from more satellites can be received, the positioning result of receiver can be very good. When it comes to between the building path, however, the receiver's output becomes unreliable and locates on the wrong side of the road. The result of GPS single point positioning is the worst among the three results. For the between buildings path, the points are nearly located all inside the buildings. Even in the intersection area, the points are outside of

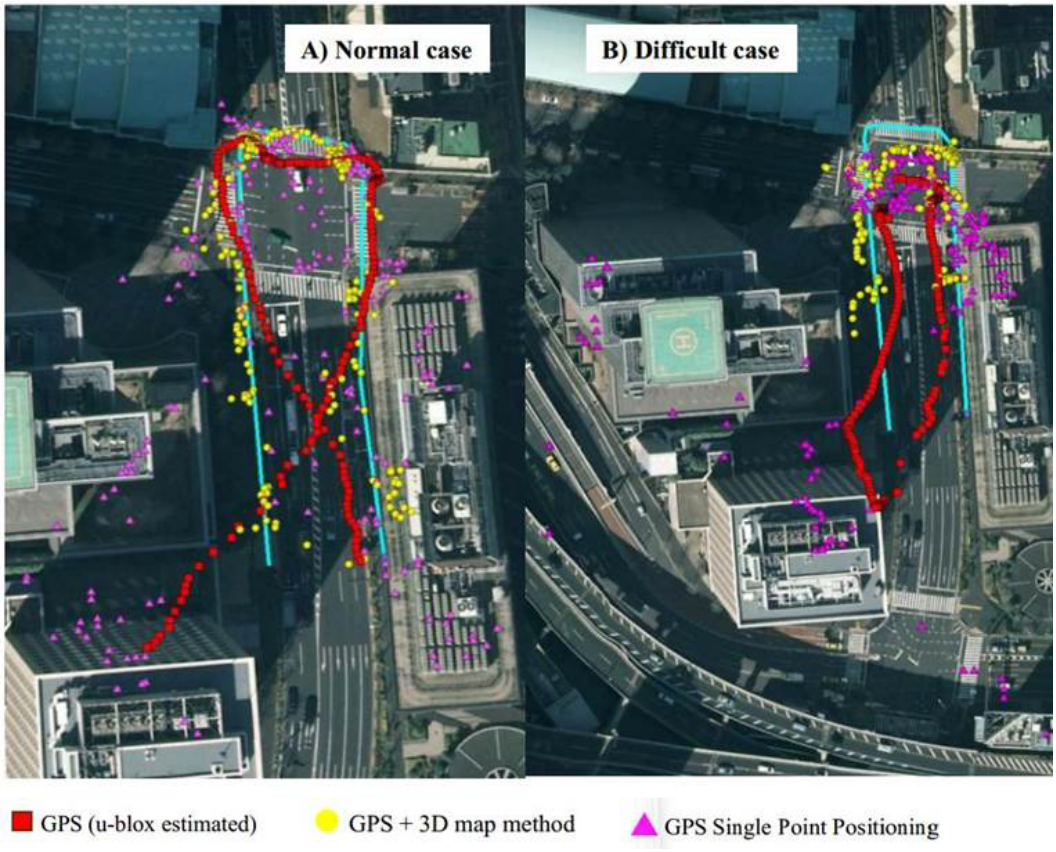

(a) The result of the receiver, 3D map method and single point positioning using only GPS

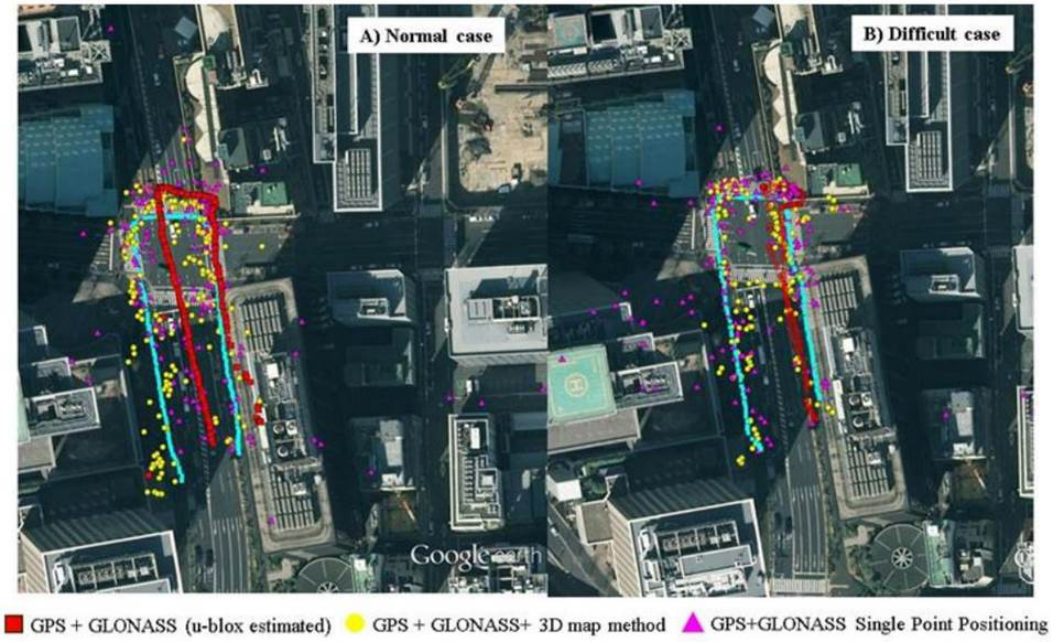

(b) The result of the receiver, 3D map method and single point positioning using GPS and GLONASS

図 3.7: The result figure of 3 different positioning methods for both GPS alone and GPS plus GLONASS

the crosswalk. For GPS with 3D map method, the result is the best among the three. At the intersection part, the result of GPS with 3D map method is similar to the result of receiver output, but at the upper part the yellow dots are more near to the cyan line. At between the buildings part, the GPS with 3D method result has fewer points than the receiver output, but unlike receiver output, the result points are on the correct side of the road.

Fig. 3.7(b) shows the result of GPS plus GLONASS with 3D map and ray tracing method. Because the usable number of satellites increases, the positioning result became much better than the GPS alone case. The result of receiver output, similar to the GPS case, is very smooth. But the result for the left path is located in the center of the road, this could be caused by the reflected signals from the satellites at the left side of the sky. For the difficult case, the result for the receiver output is totally unreliable. The points which are suppose to locate on the left side of the road happen to be on the right side, though the right side of the path seems to be good, the whole result trajectory appears to be a go and return path on the right of the road, which is totally different from what really happened. For the pink triangles, the single point positioning result, the points are very separated. At the intersetion part, most of the points are located above the ground truth and at the between buildings part, the points are either at the center of the road or far right away to the ground truth. Both way the SPP result is far from being correct. The last, the result of GPS plus GLONASS with 3D map method (yellow dots), shows the best positioning accuracy among the three methods. For both normal and difficult cases, at the intersetion part, the result follows the ground truth and at between the buildings part, the most points are locates on the correct side of the road, few points appears in the center, which is possibly caused by undetected signals and other unknown reasons.

To analyse the result statistically, the table for maximum, minimum, average error and result percentage in both normal and difficult cases is listed. The maximum, minimum and average error is simply calculated by calculating the geometric distance between the result point and ground truth point. Percentage of the result means how many points can be output during the whole experiment time when the receiver is set to output data every second. For instance, if the experiment contains 100 GPS time epoch (seconds) and one method is able to give output at 90 epoch (seconds), then the result percentage of this method is 90%. The reasons for a method unable to output a result point can be caused by insufficiency of valid satellites, the quality of signal being too low and so on.

From the table, it can be observed that for both normal and difficult cases, receiver's result can always have 100% result percentage. This is because the receiver has some kind of smoothing filter which eliminate unreliable result, compensate the no result epoch and smooth the result trajectory. For GPS SPP method, in both normal and difficult cases, the result is the worst among the three method. The result percentage, however, is better

表 3.2: Max., Min., Average bias and result percentage table for GPS and GPS plus GLONASS with SPP, receiver output and 3D map methods

Method	Max.(m)	Min.(m)	Average(m)	Percentage
Normal case				
GPS SPP	75.6	1.9	25.2	99.1%
GPS(receiver)	49.5	1.4	13.6	100%
GPS+3D	29.4	0.4	7.0	72.4%
GPS+GLO SPP	72.6	1.0	12.4	100%
GPS+GLO(receiver)	16.4	1.5	9.8	100%
GPS+GLO+3D	28.5	1.0	7.2	98.2%
Difficult case				
GPS SPP	135.7	0.4	25.2	80.3%
GPS(receiver)	31.8	5.2	20.6	100%
GPS+3D	31.6	0.4	9.0	74.3%
GPS+GLO SPP	89.3	1.0	14.2	97.2%
GPS+GLO(receiver)	22.7	1.2	12.8	100%
GPS+GLO+3D	19.0	0.0	6.0	96.6%

than 3D map method and second to the receiver output. This is because the SPP method uses all signals that it can get in the positioning process. These signals, however, contains reflected signals, multipath signals and refracted signals and they have errors. Using these signals can surely improve the result percentage but in sacrifice of the positioning accuracy. The 3D map method, however, can detect the reflected signals and calculated the errors they contain. But sometimes if a satellite is judged as a NLOS satellite and no reflection path from this satellite can be found, then this satellite is marked as inefficient and not included in the positioning process. Hence the result percentage is the lowest among the three but the positioning bias is the highest.

For both normal and difficult cases GPS with 3D map method and GPS plus GLONASS with 3D map method achieved the best positioning accuracy. In the normal case, GPS with 3D map method achieved 29.4m on max, 0.4m on min and 7.0m on average. Although the result percentage is 72.4% in normal case and 74.3% in difficult case, which is a little low, by adding GLONASS to the method, GPS plus GLONASS with 3D map method achieved 98.2% of result percentage in normal case and 96.6% in difficult case. Besides, the max of 28.5m, the min of 1.0m and the average of 7.2m in normal case and the max of 19.0m the min of 0.0m and the average of 6.0m are equal or batter than the GPS alone with 3D map method.

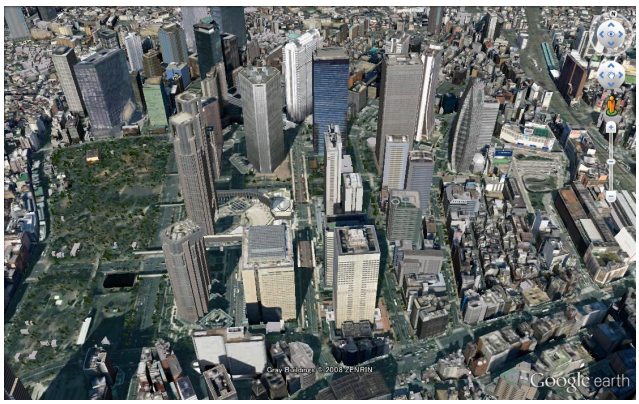

図 3.8: The experiment field as one of the deepest urban canyon area in Tokyo

3.3.3 Simulation of Valid Satellite

Moreover, a simulation has been done using the 3D map and the ray tracing method. To visualize the change of the number of the valid satellite after using 3D map method and adding GLONASS into the method, the area of Shinjoku of Tokyo is selected as the experiment field of the simulation because this area has one of the deepest urban canyon are in Tokyo. Fig. 3.8 shows the building geometric layout of the experiment field.

Fig. 3.9 shows the simulation result. In the simulation, the number of the valid satellites is display by color. And the color bar which shows what color shows what number is on the right side of the figure. There are 4 subfigures in the figure, each means the number of valid satellites in GPS only method, GPS with 3D map method, GPS plus GLONASS method and GPS plus GLONASS with 3D map method.

In the simulation, the definition of valid satellite is LOS satellite. We suppose the receiver is located on a known coordinate and the coordinate of satellites can also be calculated using the ephemeris data. For instance, if we want to known the number of valid satellite at 10:00:00 on Janurary 1st, 2014, all we need to do is to download the ephemeris data of GPS and GLONASS and calculate all the satellite position at that specific time. After that the ray tracing process can be applied. In GPS and GPS plus GLONASS method, the valid satellite is defined as LOS satellite, which means if a line segment connecting the point and the satellite is cut of by any building plane, then the satellite is invalid, otherwise valid. For GPS with 3D map method and GPS plus GLONASS with 3D map method, the definition for valid satellite is different. A valid satellite can be, firstly a LOS satellite just as in GPS and GPS plus GLONASS method, or secondly a NLOS satellite with at least one reflection path is detected.

From the simulation result, it is clear that for GPS only method, for most of the area

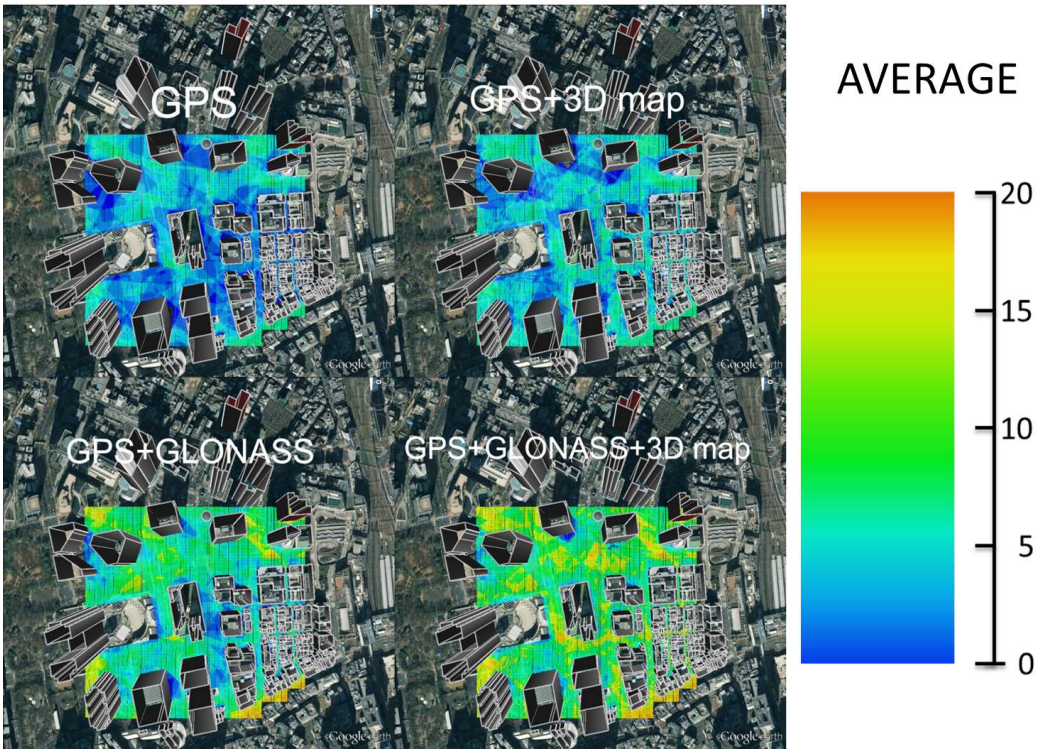

図 3.9: Simulation of the number of valid number of satellites of Shinjuku area

in the experiment field, the valid satellite number is under 5, which means no reliable position can be calculated using only GPS. The GPS with 3D map method increases the number of valid satellite in most of the blue areas in GPS only figure. The average valid satellite number in GPS with 3D map method is around 5. After adding another 24 satellites in the orbit, the GPS plus GLONASS method significantly increases the valid satellite number. At some relatively open area, the valid satellite number can even reach 15, but at between the building area, there are still some regions displayed as blue, with valid satellite number below 5. The last subfigure shows the simulation result of GPS plus GLONASS with 3D map method. As can be observed, there are basically no blue regions in this method, for most of the part the color is green, which means the valid number of satellite is around 10. For some open areas, this number can even climb up to above 20.

In conclusion, by adding GLONASS into GPS with 3D map method, the positioning accuracy is increased, the experiment show that the average positioning bias is 7.2m in normal case and 6.0m in difficult case. And the result percentage also greatly increased from 72.4% to 98.2% in normal case and 74.3% to 96.6% in difficult case. Besides, the number of valid satellites for GPS plus GLONASS with 3D map method is the most, around 10 on average. Even in one of the deepest urban canyon area in Tokyo, the GPS plus GLONASS with 3D map method can always give reliable result.

第 4 章

Multipath Correlator for Multipath Mitigation

As introduced in the former chapters, one of the reasons that satellite-based positioning system can not give reliable positioning result in urban area is because of the buildings can reflect signals. And when a line segment connecting the receiver and a satellite is cut off by a building plane, then this satellite is NLOS and the only signal that can reach the receiver from this satellite is a reflected signal. But what is the line segment is not cut off by any building planes and a reflection path is also detected? In this case, we call this satellite a multipath satellite, as Fig. 4.1.

4.1 A Brief Introduction of Multipath Correlator

In the multipath case, since the reflected signal covers longer distance than the direct signal, the reflected path must reach the receiver later than the direct signal. According

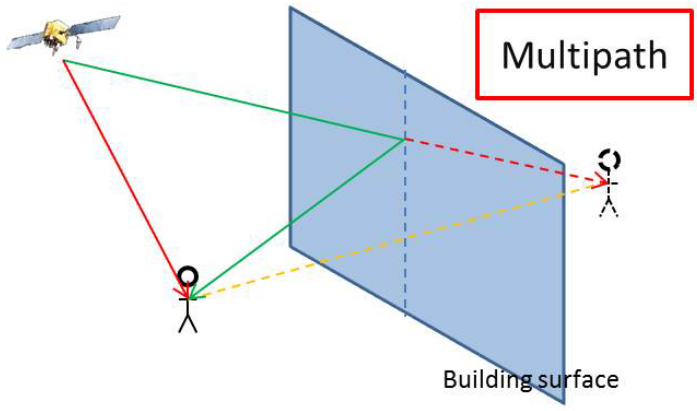

図 4.1: An illustration of a multipath satellite - when LOS signal and reflected signal both reach the receiver

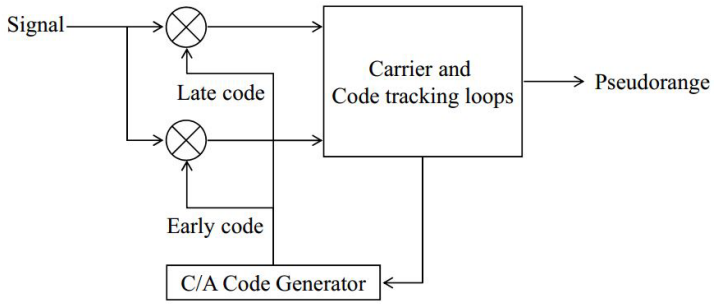

図 4.2: The delay lock loop mehod used inside the receiver to decide the receive timing

to [**?**, **?**] when the reflected signal is later than the direct signal for 1.5 chip of C/A code, this reflected path would have little influence on the receiver. However, when the reflected path is reflected by some objects near to the antenna, which makes the arrival delay very small, then the receiver would be unable to eliminate this reflected signal. And the error caused by this reflected signal is called multipath error. In this case, the length of the reflected path is not the same as the measured pseudorange. To solve this relationship, the multipath correlator is needed.

Inside the receiver, the method used to decide the receive time of a signal from a satellite is called Delay Lock Loop (DLL), as illustrated by Fig. 4.2. The methodology will be introduced at the following part.

The DLL firstly generate 2 replica signal of the a specific signal from a satellite. One replica is a little early and the other is a little late. The difference between these two signals are 1 chip. After that, the correlation of the the 2 replica signals with the received signal are examined. And adjust the 2 replica signals to the relationship between the received signal and each of them the same. And when the relationship are the same, the time at the center is set as the signal received time. This whole procedure is listed in Fig. 4.3(a) and (b).

This is the most basic function of the correlator. But when a reflection is involved in the received signal, for example, the signal strength is 0.3 time of the direct signal and the delay is 0.2 chip, as shown in Fig. 4.4.

As can be observed, with the involvement of the red multipath signal, the position of the early and late position are change, about 0.1 chip later than the original direct path signal correlation. Since 1 chip means 978ns and about 293m, 0.1 chip will cause 29.3m error in the calculation of the measured pseudorange, which will in turn cause positioning error when used in the weighted least square method.

In order to solve the error caused by the multipath signals, many methods have been proposed. For instance, [15] proposes to only modify the relation factors inside the receiver

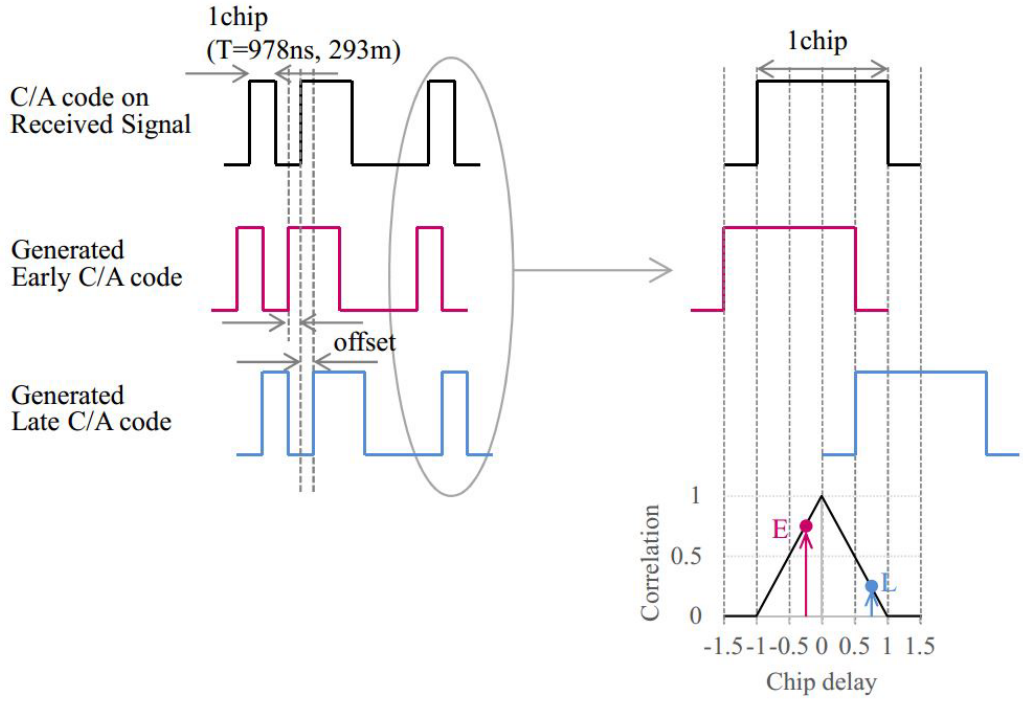

(a) The result of the receiver, 3D map method and single point positioning using only GPS

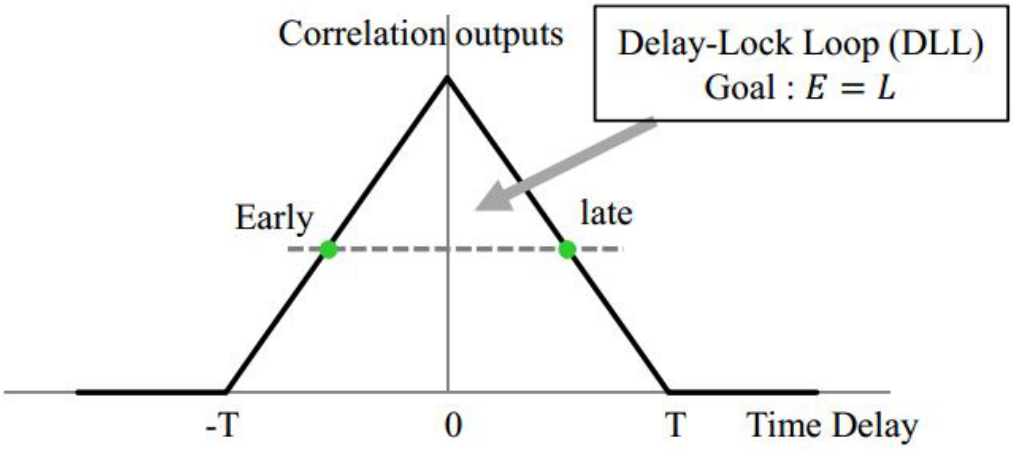

(b) The result of the receiver, 3D map method and single point positioning using GPS and GLONASS

図 4.3: The result figure of 3 different positioning methods for both GPS alone and GPS plus GLONASS

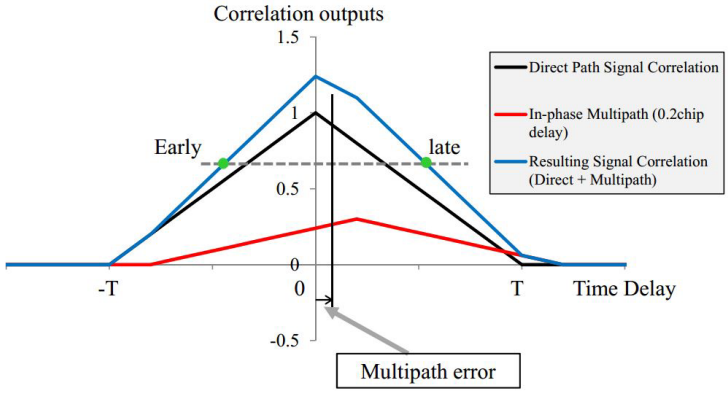

図 4.4: The example of involving a multipath signal of 0.3 time of the strength and 0.2 chip delay

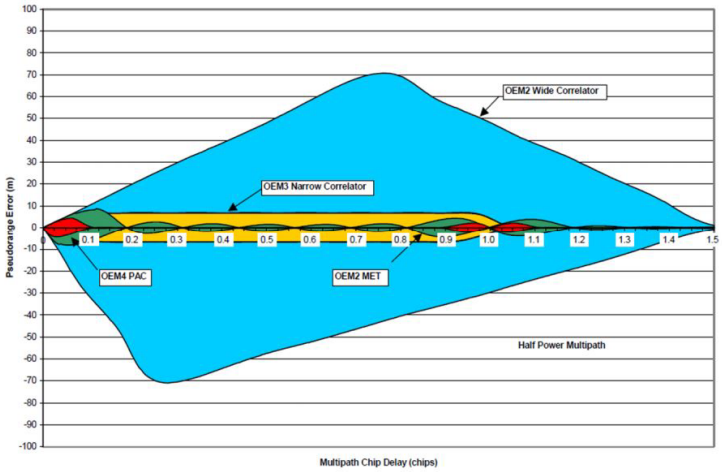

図 4.5: The relationship between pseudorange error and multipath chip delay

to refer the error when the delayed distance is unknown. With 3D map and ray tracing algorithm, however, the length of the reflected path can be calculated, hence the distance difference between the LOS signal and reflected signal can be computed. In this case, using the relationship between the delay distance and multipath bias can be helpful.

[**?**] showed this relationship between the pseudorange error and multipath chip delay, as shown in fig. 4.5. This relation ship is called the multipath correlator and usually, there are wide correlator, narrow correlator, pulse aperture correlator and so on. In Miura's work, the multipath correlator is displayed in Fig. 4.6, the x-axis means the distance difference, which is calculated by chip multiple the distance of one chip.

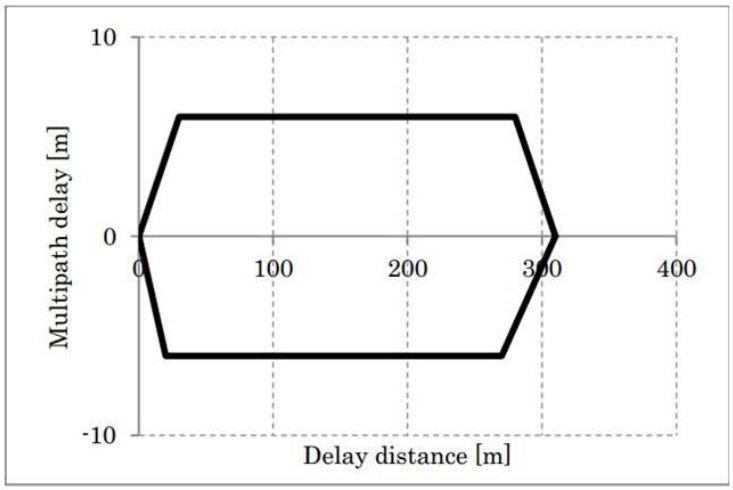

図 4.6: The multipath correlator used in Miura's method

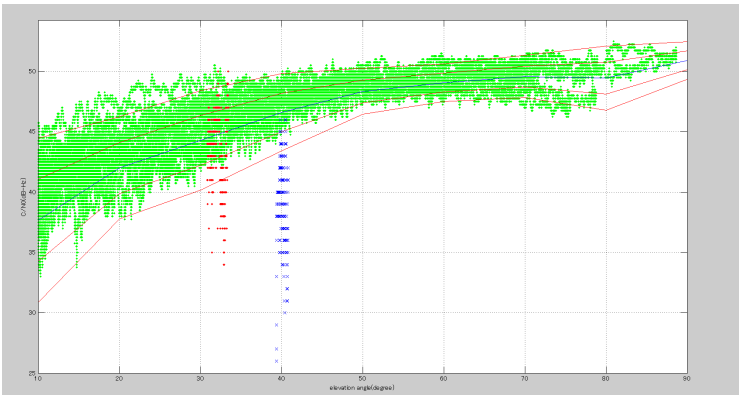

図 4.7: The relationship between elevation angle, signal strength and the examples of two multipath signals

4.2 Material-based Multipath Correlator

Since the receiver used in Miura's work was u-blox6, which can only receive GPS signals. As introduced above, the receiver used in this thesis is u-blox8, an upgraded version of the u-blox6 receiver. And besides, in the experiment, we found one fact that different with the common concept of higher elevation angle, stronger signal strength, some time the multipath signals have stronger signal strength with lower elevation angle, as shown in Fig. 4.7.

In this figure, the y-axis means signal strength (dB-Hz), and x-axis means elevation angle. The green points are generated from the data collected on the top of IIS, where is a totally open sky environment. This also means that no multipath signal is inside. The

trend of the green points follow the rule of the higher the elevation angle, the stronger the signal strength.

The red and the blue points, however, are generated from data collected in urban area. And with the 3D map and ray tracing algorithm, we can decide that these two signals are multipath signals. Fig. 4.8 shows the ray tracing result of the both cases.

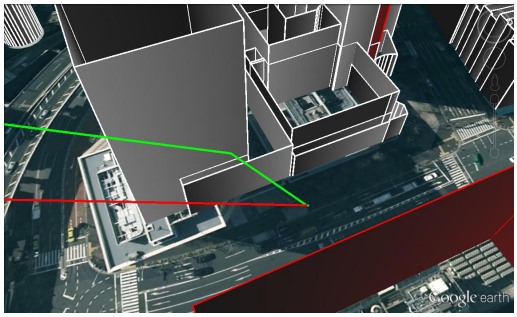

(a) Ray tracing result with concrete wall as the reflection surface

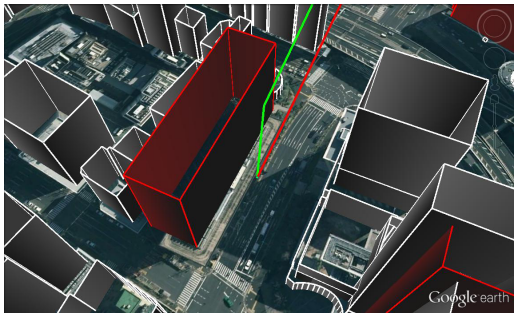

(b) Ray tracing result with glass wall as the reflection surface

図 4.8: Ray tracing result with the reflection surface of concrete and glass

In the figure, the red building means a building with glass surface and grey building means a building with concrete surface. The method of deciding the material of the building is based on visual check. Since the signal strength is not obeying the common concept of the higher elevation angle, the stronger the signal strength and both of these signals are influenced by multipath, we made an assumption that the reflection surface, namely the material of the reflection surface can affect the multipath error, hence compared to the common method which uses only one multipath correlator for all multipath signals, we propose to use a material-based multipath correlator to deal with the reflected signals with different type of reflection surface.

Fig. 4.9 shows the 3D map of Hitotsubashi area with the building material labelled. The red buildings means the buildings that have glass surfaces and grey buildings the buildings that have concrete surfaces.

4.3 Generation of the Material-based Multipath Correlator through Experiments

To generate the material-based multipath correlator for glass and concrete, we have to firstly make sure that the signal is a multipath signal and the material of the reflection surface is glass or concrete. Fortunately, 3D map and ray tracing method provide a way of knowing these.

Firstly, at the Hitotsubashi experiment field, several points are picked, from which a

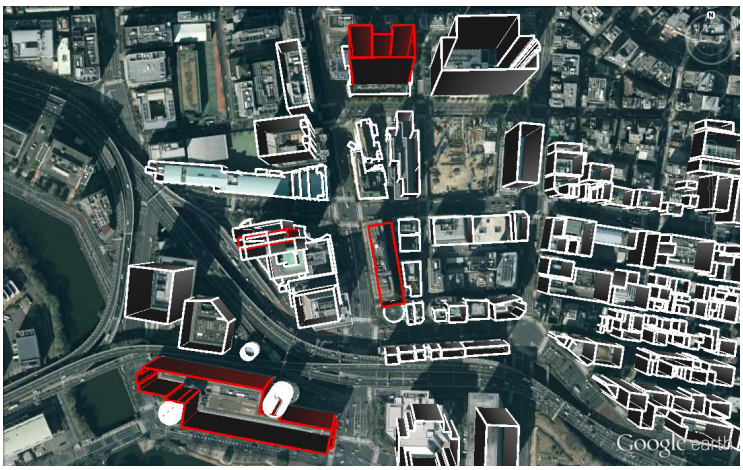

図 4.9: The 3D map of Hitotshbashi area with the building material labelled

multipath signal is easy to receive. Fig. 4.10 shows these points.

At each point, a data set of an interval of 5 minutes are collected. And with the correct satellites layout, one or two multipath signal can be picked by the receiver, as illustrate by Fig. 4.11 as one case of one multipath signal with a concrete reflection surface. Besides, the signal strength of this signal is also examed, as shown in Fig. 4.12, the signal strength varies a lot compared to the data collected in open sky area, which proves that the signal must be a multipath signal.

And after that we can be sure that this signal, as illustrated as one signal from GPS 9 satellite, is a multipath signal and getting data concerning this signal. The most important data in this case is the measured pseudorange and the direct and reflected path from the satellite to the point. When the parameters are collected, a figure like Fig. 4.13 can be generated, with the equation for x-axis is

$$d^{multipath} = d^{reflected} - d^{direct}$$

and the equation for y-axis is

$$\varepsilon^{pseudorange} = meaR - simR$$

where $d^{multipath}$ denotes the multipath delay, $d^{reflected}$ denotes the length of reflected path and d^{direct} the length of the direct distance from the point to the satellite, $\varepsilon^{pseudorange}$ denotes the pseudorange error and $meaR$ and $simR$ mean the measured pseudorange and simulated pseudorange respectively.

Based on the methodology introduced above, the multipath correlators for both concrete and glass material can be generated.

As can be observed from the figure, in (a) of Fig. **??**, the multipath correlator for concrete surface, when the multipath delay is about 15m, the it can cause the pseudorange

図 4.10: Points of data collection

error upto 6.2m and when the multipath delay is bigger than 32.0m, the pseudorange doesn't be effected. Same results can be observed from the multipath correlator for glass surface, where the biggest error in pseudorange of 12.2m happens when the multipath delay is about 10m long, and when the multipath delay exceeds 13.0m the reflection path can not affect the pseudorange.

4.4 Experiment Results for Material-based Multipath Correlator

To prove the efficiency of the material-based multipath correlator, experiments are conducted at Hitotsubashi area. Fig. 4.14 shows the result of the experiment. There are two sets of data used collected and the material-based multipath correlator is evaluated based on these two sets of data.

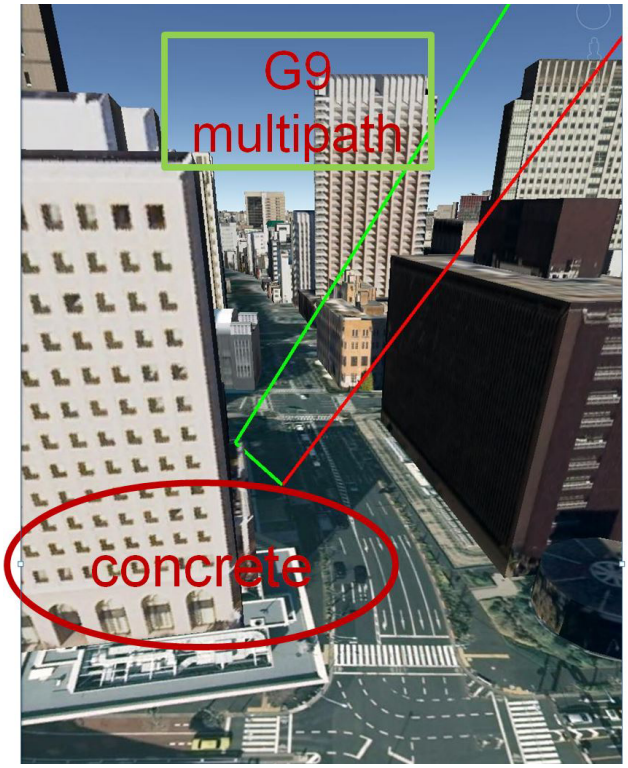

図 4.11: One example of detecting a multipath signal with a concrete reflection surface

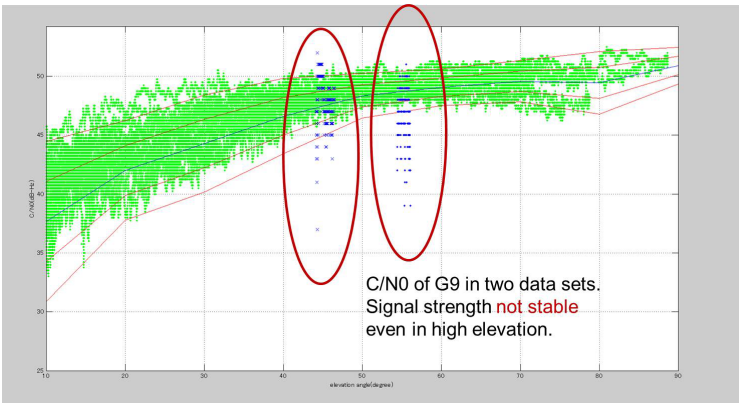

図 4.12: The signal strength of G9 satellite compared to the data collected in open sky area

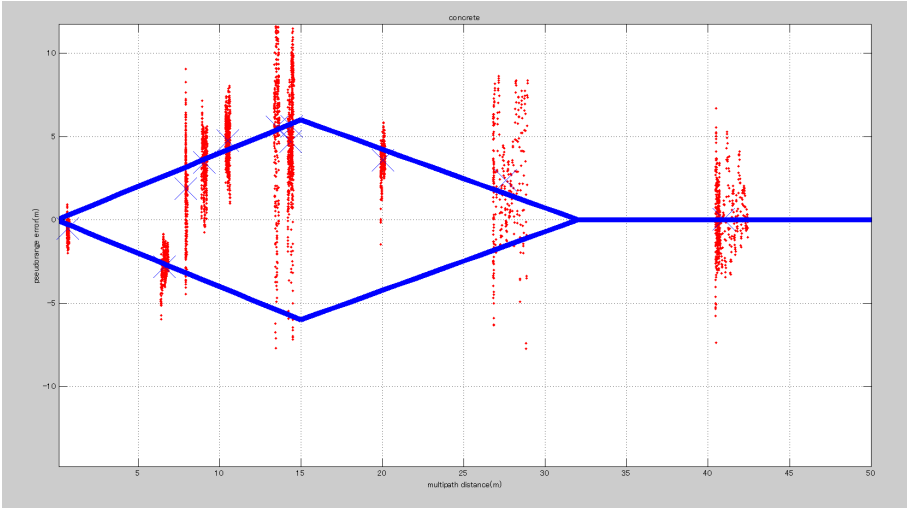

(a) The multipath correlator for concrete surface

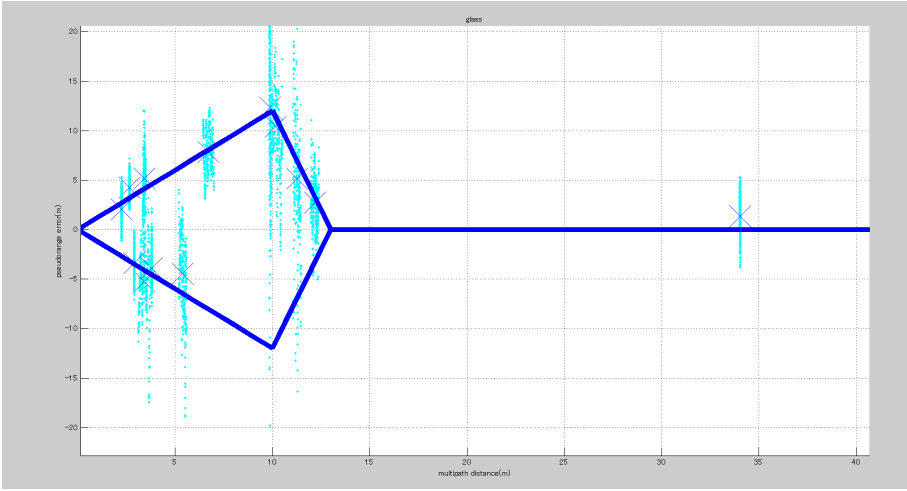

(b) The multipath correlator for glass surface

図 4.13: The material-based multipath correlator for both concrete and glass

In the result, the green dots denotes the ground truth, the red dots is the result using the new material-based multipath correlator and the cyan dots means the result of the old multipath correlator. As can be observed, the result using new material-based multipath correlator is clearly better than the old one. Especially on the right side of the road under a building with glass surface, in data set 1, the red dots are nearer to the ground truth than the cyan dots and in data set 2, the red dots are more dense and have an incline to ground truth than the cyan dots.

The following table is the statics of the results of the two data sets. The maximum, minimum and average error of the results are displayed. It is clear from the table that with the material-based correlator, the average error in improved by about 1m, which

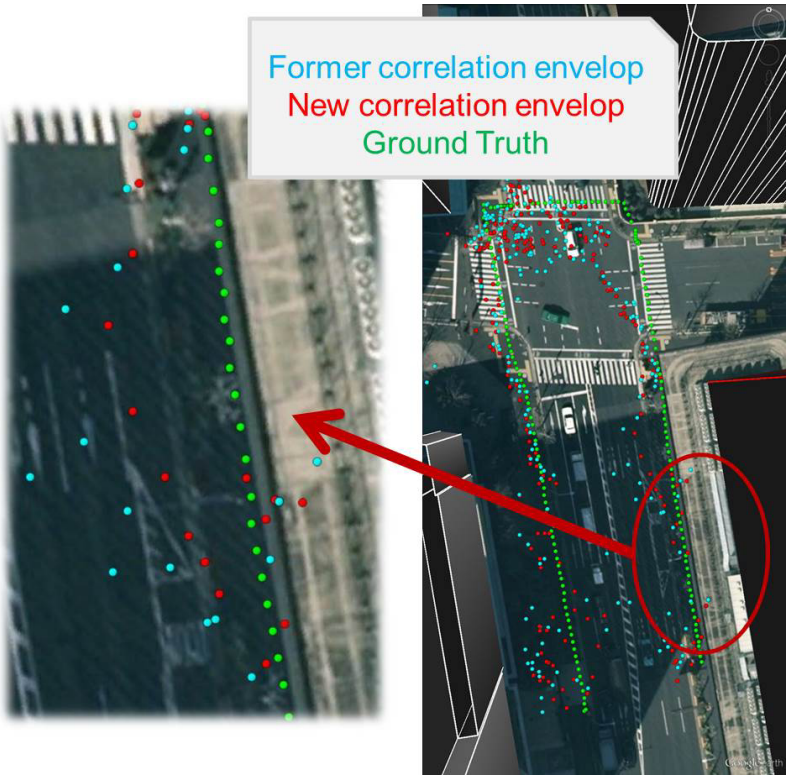

(a) The result of data set 1

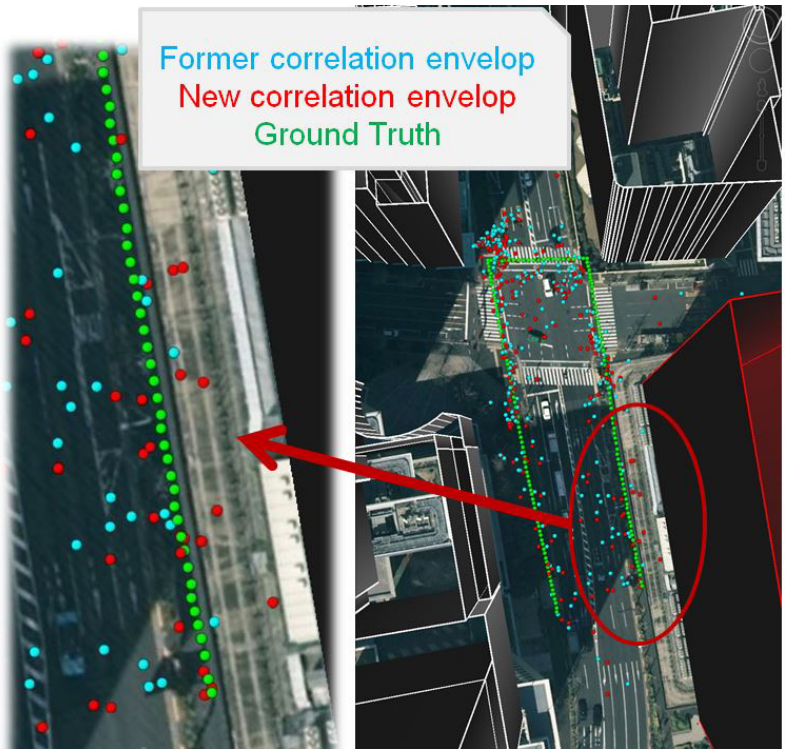

(b) The result of data set 2

図 4.14: The material-based multipath correlator for both concrete and glass

表 4.1: The Max. Min. and average error of the result using the old multipath correlator and the new material-based multipath correlator

Method	Max.(m)	Min.(m)	Average(m)
Data 1			
Old correlator	27.12	0.14	4.26
Material-based correlator	10.44	0.15	3.22
Data 2			
Old correlator	36.88	0.11	4.28
Material-based correlator	24.19	0.05	3.71

proves the efficiency of the material-based multipath correlator.

第 5 章

The Double Reflection Algorithm

In the chapter above, 3D map and ray tracing method was introduced. To some deep urban environments, especially in Japan where the roads are narrow and buildings are high, second time reflections are probable. Thus a second reflection detection algorithm is developed to detect any possible second time reflections.

In this chapter, the logic of the second time reflection algorithm will be presented and a result using the second time reflection algorithm will also be analysed.

5.1 The Double Reflection Detection

Similar to the single time reflection detection algorithm, the second time reflection detection algorithm is also based on the calculation of the mirror positioning and the reflection points on the plane. Fig. 5.1 shows the concept figure of the detection algorithm.

As can be observed, the solid line human figure means the position of the sample point, namely the receiver possible position. Firstly, same to the single time reflection algorithm, a mirror point, mirror 1 is calculated based on the a plane, plane 1, and secondly, another mirror point, mirror 2, based on mirror 1 and another plane, plane 2, is calculated. After this, 4 coordinates can be acquired, the sample point, mirror 1 point, mirror 2 point and satellite point.

In order to make the reflection path possible, several premises must be satisfied at first. If we assume that the plane, plane1 and plane2, are infinitely large and each of them divides the whole space into two spaces, the one on the right and the other one on the left. And to plane1's two spaces, the mirror2 and sample point must be on the same right or left space and to plane2's two spaces, the mirror1 and satellite point must on the same right or left space. Only by satisfying these premises can a second time reflection path be geometrically possible.

In Algorithm. 3 listed proposed the second time reflection detection algorithm.

Different to the one time reflection detection algorithm, there are three line segments

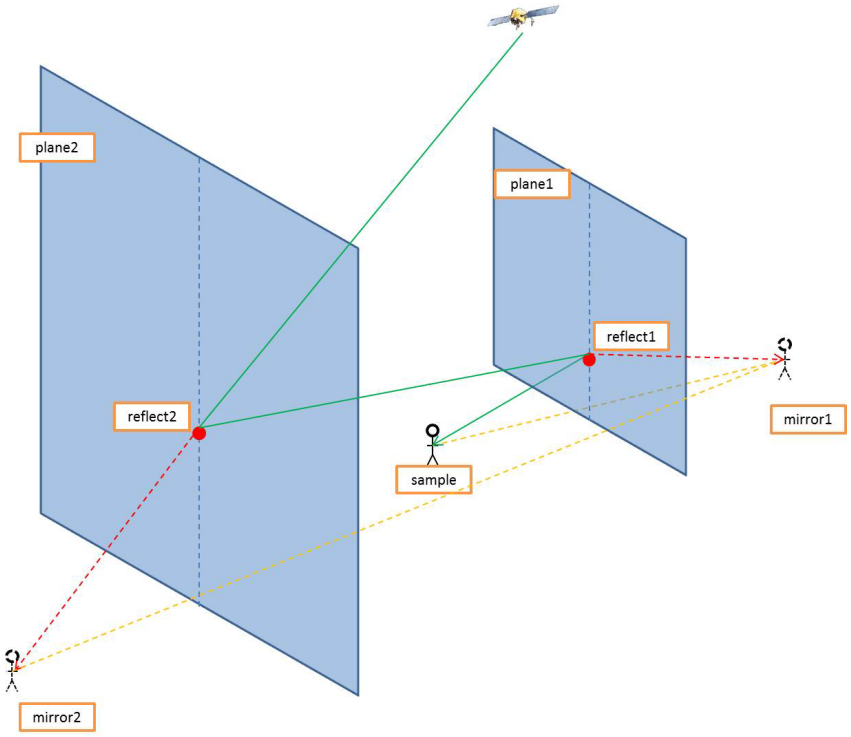

図 5.1: The procedure for the Double reflection detection

need the cut-off detection. And the reflection possibility check is based on two planes instead of only one plane. Accordingly, these differences can cause many new problems and the following section will introduce the most significant one.

5.2 Computation Load

The most difficult problem in the second time reflection detection algorithm is the computation load. In the algorithm, there are a storage space used to store all possible reflection combinations of satellite, plane and sample point. The number of this combination affects processing time greatly. And by analysing this number, the computation load can be estimated.

For instance, if the 3D map contains 100 buildings and each building contains 4 planes, then in one time reflection detection, to every sample point, 400 planes will be checked.

In the double reflection scenario, however, in the same 400 planes case, there are 400 x 400 combination of planes needed to be checked. And at most of the time, there are much more buildings than only 100 and every building have at least 4 planes. Which means the computation load will be much larger that one time reflection case. For example, in one data collected at Hitotsubashi area, the computation load increases from 141 to 128619 when the double reflection detection is applied. Moreover, the acture time consumed by

Algorithm 3 The detection of a Double reflection path

```
Calculate the mirror1 position (dashed line human figure) of a fixed ground point (solid line human figure) to a known plane1.
Calculate the mirror2 position of the mirror1 point to a known plane2.
if To plane1, mirror2 and the fixed point are on the same side and to plane2, mirror1 and satellite are on the same side. then
    Connect the satellite and the mirror2.
    Detect the crossing point (reflect2) of the line and the plane2.
    Connect the reflect2 and the mirror1.
    Detect the crossing point (reflect2) of the line and the plane1.
    if Reflect1 and reflect2 both exist. then
        Connect satellite with refl2ct2, reflect2 with reflect1 and reflect1 with sample.
        if The 3 line segments are not cut off by any other plane. then
            The double reflection path exist.
        else
            The double reflection path doesn't exist.
        else
            The Double reflection path doesn't exist.
        end if
    end if
else
    The Double reflection is not possible.
end if
```

one time reflection detection is about 1 second per GPS epoch, but when detecting the double reflection, the time consumption is more than 5 minutes per GPS epoch, which is totally unacceptable to be used in online positioning scenario.

In order to minimize the computation load and accelerate the processing speed, we set the first and second reflection plane and only detect the double reflection generated by these two planes, as Fig. 5.2 illustrates.

5.3 Experiment Result

Experiments have been conducted in Hitotsubashi area to test the efficiency of the double reflection algorithm. Fig. 5.4 show the ground truth of the experiment and GPS epoch from 263447 to 263450 (points in the white rectangular) of this data are mainly examed because of the computation load is too high.

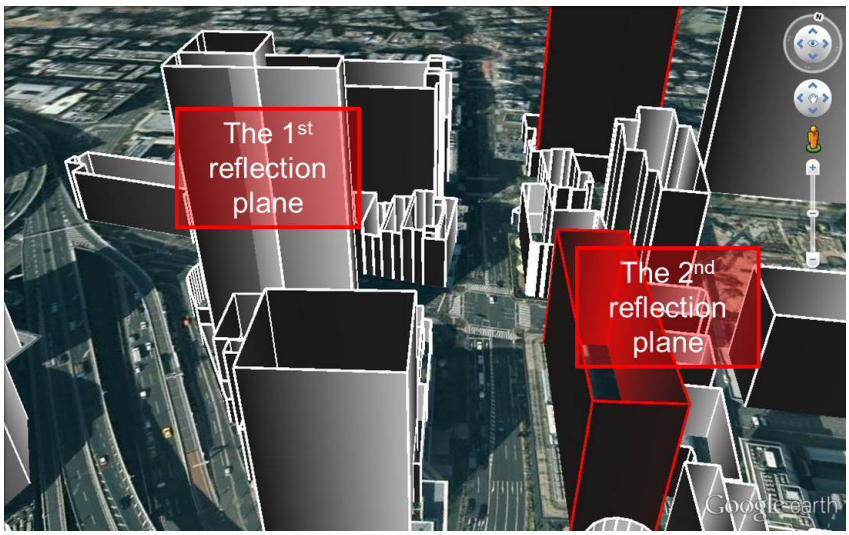

図 5.2: Label the reflection plane for double reflection to minimize computation load

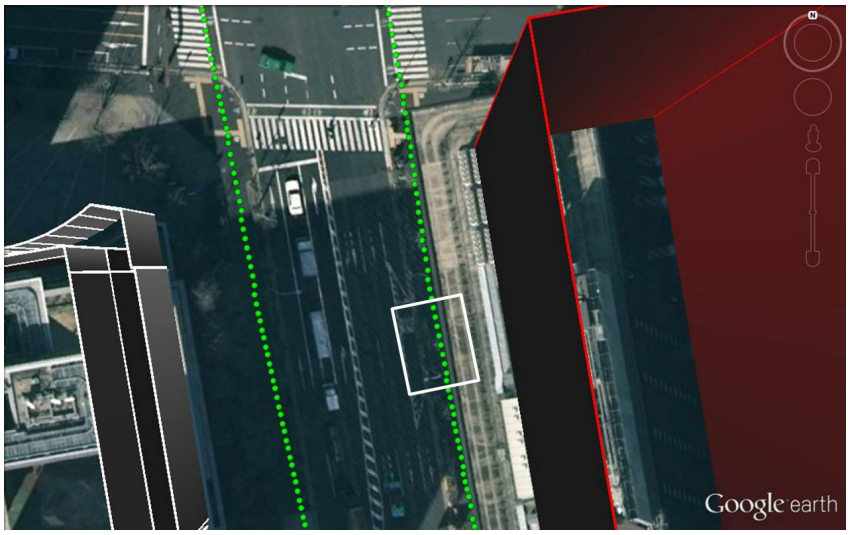

図 5.3: Only several GPS epoch are processed with double reflection detection

To these several GPS epoch, both one time reflection and double reflection algorithm are applied. Fig. 5.4 shows the result of these epoch. The green dots are ground truth, the cyan dots are the result of the one time reflection and red dots are the result of double reflection. To illustrate, besides detecting double reflection in the red dots, one time reflection is also applied, but when a satellite and a sample point pair has both one time reflection and double reflection, the double reflection is used priorly.

For a NLOS satellite, if a one time reflection is found then this satellite is judged as valid, but when the double reflection algorithm is applied, this satellite is valid if either a one reflection path or a double reflection path is found. And when both kinds of reflection

are found, the double reflection is used priorly in the red dots.

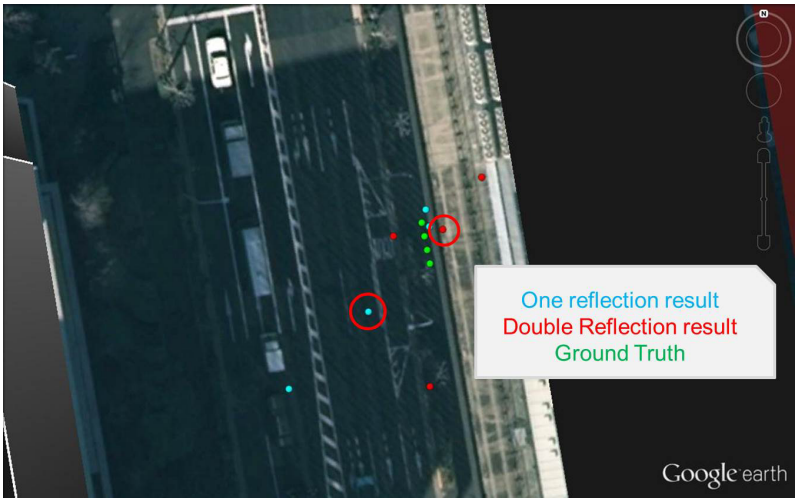

(a) The result of one and double reflection

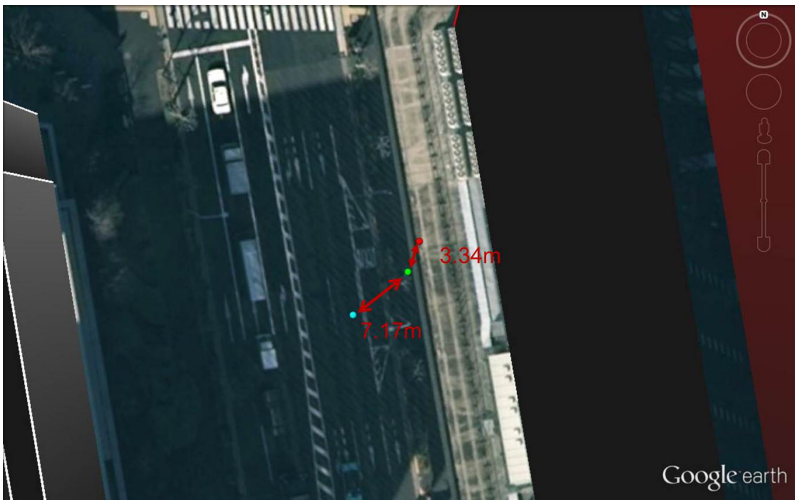

(b) Focus on GPS epoch 263450 of the data

図 5.4: The material-based multipath correlator for both concrete and glass

As can be observed, in the double reflection result, some times the result is better than that of the one reflection result, sometime it is not. And in order to analyse in which case the result can become better, a specific GPS epoch, 263450, is selected, as shown in the red circle of (a) of Fig. 5.4.

In Fig. 5.4 (b), the statistic is listed. The result of double reflection (red) is 3.34m away from the ground truth but the result of one reflection (cyan) is 7.17m, which means the double reflection is more accurate in this epoch. Fig. 5.5 shows the ray tracing result of satellite G32, which is a NLOS satellite and no one reflection but only one double reflection path is found. In this case G32 is judged as valid in the program and used to

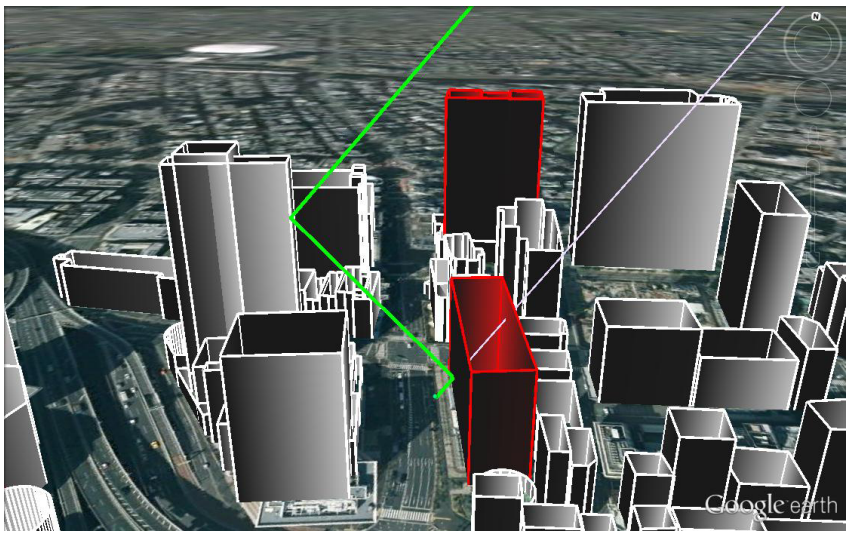

図 5.5: The double reflection from satellite G32

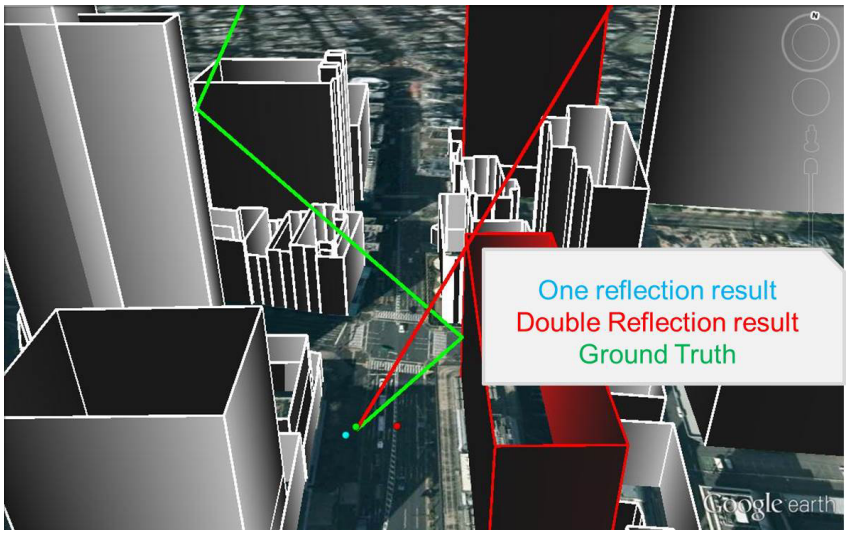

図 5.6: A multipath satellite with a double reflection detected

calculate the similarity. We believe this is the reason why the double reflection result at this GPS epoch is better than the one reflection result.

However, sometime the double reflection can make the result worse. Fig. 5.6 demonstrates such an example. In this case, no one reflection can be found but a double reflection with a direct path are found. And applying this ray tracing result to the program made the positioning result go bad. As the red point was located in the middle of the road while the cyan point is much nearer to the ground truth.

In conclusion, the double reflection algorithm can sometimes increase the positioning accuracy and at the other times decrease the positioning accuracy. Hence a reflection

judging algorithm should be developed, which can decide when and how to use the detected double reflection to make the result more accurate.

第 6 章

Conclusion and Future Work

This thesis presents an improved version of 3D map and ray tracing positioning method for pedestrian in urban area.

Firstly, adding another GNSS, GLONASS, into the GPS with 3D map method increases the number of usable satellite dramatically. Experiments and simulation are conducted to prove the efficiency of this multi-GNSS with 3D map method. The experiment in Hitotsubashi area proved that the positioning accuracy and result percentage are both increases with the help of GLONASS. And simulation in Shinjoku area also shows the number of usable satellites is double compared to the GPS alone method.

Secondly, a sophisticated material-based multipath correlator designed to solve the multipath problems caused by various building surfaces is proposed and tested. The multipath correlator is designed for concrete and glass surfaces. With the assistance of 3D map, the surface that causes the reflection can be recognized and if the signal is multipath signal, the concrete and glass correlators can be applied to mitigate the multipath error. To prove the efficiency of the sophisticated material-based multipath correlator, experiments are conducted at Hitotsubashi area. The positioning accuracy, concerning max, min and average error, is increased.

Thirdly, an improved ray tracing algorithm is proposed to ray trace the double reflection. Although double reflection detection can be used in some cases, it sometimes makes the positioning result worse. Also experiments are performed to test the algorithm. In the several GPS epoch time, some epoch are better but the others went worse. Hence a judging algorithm which can decide the reliable of the double reflection should be developed.

In the future, several other improvements to the 3D map method can be researched. For instance, adding another GNSS, for example BeiDou or GALILEO, can be added to the current method so that more satellites can be used. And besides concrete and glass, there exist other types of buildings which can affect the multipath error hence more correlators can be developed. And for the double reflection algorithm, a reliability judgement algorithm can be proposed.

Thanks

This thesis is under the instruction of Professor Kamijo, who gave me directions, advices on not only the researches but also all aspects of my life.

Ms. Miwa, Professor Kamijo's secretary, also provided huge help to my research life in the lab.

Also researcher Gu and Qmo are beacons that lighted my way forward. Nothing in this thesis can be achieved without their help. To the other members in the lab, Sunagawa, Wada, Hashimoto, Huang, Bao, Liu and Mahdi, I want to thank them for companying me through the 2 years and make all these time more meaningful tome.

Lastly, I want to thank my family and friend for their supporting my research work.

2014 年 2 月 5 日

発表文献

Society of Automotive Engineers of Japan

[1] Feiyu Chen, Li-Ta Hsu, and Shunsuke Kamijo, "Evaluation of Multi-GNSSs and GPS with 3D Map Methods for Pedestrian Positioning in an Urban Canyon Environment," JSAE Annual Congress (Autumn), Oct. 2014.

Reference

[1] G. MacGougan, G. Lachapelle, R. Klukas, K. Siu, L. Garin, J. Shewfelt, and G. Cox, "Performance analysis of a stand-alone high-sensitivity receiver," *GPS Solutions*, vol. 6, no. 3, pp. 179–195, 2002.

[2] S. H. Shunsuke Miura and S. Kamijo, "Gps positioning with multipath detection and rectification using 3d maps," *ITS World Congress*, 2013.

[3] F. Peyret, D. Btaille, M. Ortiz, S. Miquel, and L. Fontenay, "How to improve gnss positioning quality of service for demanding its in city environments by using 3d digital maps," in *19th ITS World Congress, Vienna, Austria, 22-26 October*, 2012.

[4] 坂井　丈泰, "Gps のための実用プログラミング," 2008.

[5] E. D. Kaplan and C. J. Hegarty, *Understanding GPS: principles and applications*. Artech house, 2005.

[6] W. Feess and S. Stephens, "Evaluation of gps ionospheric time-delay model," *Aerospace and Electronic Systems, IEEE Transactions on*, no. 3, pp. 332–338, 1987.

[7] J. Saastamoinen, "Atmospheric correction for the troposphere and stratosphere in radio ranging satellites," *Geophysical Monograph Series*, vol. 15, pp. 247–251, 1972.

[8] B. Hofmann-Wellenhof, H. Lichtenegger, and J. Collins, "GPS theory and practice," 1997.

[9] P. Lindner and G. Wanielik, "3D LIDAR processing for vehicle safety and environment recognition," in *Computational Intelligence in Vehicles and Vehicular Systems, 2009. CIVVS '09. IEEE Workshop on*, 30 2009-april 2 2009, pp. 66 –71.

[10] 小島祥子, 高橋新, and 二宮芳樹, "汎用 gps と車載レーザレーダを用いた高精度自車両位置推定," **情報処理学会論文誌**, vol. 50, no. 1, pp. 64–74, 2009.

[11] L. Jin, Q. Niu, H. Hou, H. Shunxi, and W. Fangrong, "Study on vehicle front pedestrian detection based on 3D laser scanner," in *Transportation, Mechanical, and Electrical Engineering (TMEE), 2011 International Conference on*, dec. 2011, pp. 735 –738.

[12] K. R. J. S. G. A. Mcgraw, R. S. Y. Young and F. Ventrone, "Gps multipath mitigation assessment of digital beam forming antenna technology in a jpals dual frequency smoothing architecture," *Proceedings of the 2004 National Technical Meeting of the*

Institute of Navigation, pp. CA 561–572, 2004.

[13] P. F. A. J. Van Dierendonck and T. Ford, "Theory and performance of narrow correlator spacing in a gps receiver," *Navigation*, vol. 39, no. 3, pp. 265–283, 1992.

[14] J. M. N. Viandier, D. F. Nahimana and E. Duflos, "Gnss performance enhancement in urban environment based on pseudo-range error model," *osition, Location and Navigation Symposium, 2008 IEEE/ION*, no. 3, pp. 377–382.

[15] 久保信明, 安田明生, and 鈴木崇史, "衛星測位におけるマルチパス誤差の削減と高精度化への可能性について," **電子情報通信学会技術研究報告** *(ITS* **研究会***)* **資料**, **信学技報**, vol. 104, no. 230, p. 12, 2004.

[16] 土本和彦, 久保信明, 海老沼拓史, and 安田明生, "反射波が支配的な状況下でのマルチパス誤差低減," **日本航海学会論文集**, no. 118, pp. 221–227, 2008.

[17] R. G. Brown, "A baseline gps raim scheme and a note on the equivalence of three raim methods," *Navigation*, vol. 39, no. 3, pp. 301–316, 1992.

[18] Y. C. Lee and D. G. O' Laughlin, "A performance analysis of a tightly coupled gps/inertial system for two integrity monitoring methods," *Proceedings of ION GPS, Nashville*, pp. 14–17, 1999.

[19] T. Iwase, N. Suzuki, and Y. Watanabe, "Estimation and exclusion of multipath range error for robust positioning," *GPS solutions*, vol. 17, no. 1, pp. 53–62, 2013.

[20] N. Kubo, T. Suzuki, A. Yasuda, and R. Shibazaki, "An effective method for multipath mitigation under severe multipath environments," in *Proceedings of the 18th International Technical Meeting of the Satellite Division of The Institute of Navigation (ION GNSS 2005)*, 2005, pp. 2187–2194.

[21] M. Obst, S. Bauer, P. Reisdorf, and G. Wanielik, "Multipath detection with 3D digital maps for robust multi-constellation GNSS/INS vehicle localization in urban areas," in *Intelligent Vehicles Symposium (IV), 2012 IEEE*, june 2012, pp. 184 –190.

[22] H. L. Bertoni, *Radio propagation for modern wireless systems*. Pearson Education, 1999.

[23] M. F. Iskander and Z. Yun, "Propagation prediction models for wireless communication systems," *Microwave Theory and Techniques, IEEE Transactions on*, vol. 50, no. 3, pp. 662–673, 2002.

[24] D. Vorontsov, "Glonass nearing completion," *Russia and CIS Observer*, 2010.11.26.

[25] ——, "The global navigation system glonass: Development and usage in the 21st century," *34th Annual Precise Time and Time Interval (PTTI) Meeting*, 2002.

[26] Dominic, "What is the difference between satellite navigation systems gps and glonass?" *http://www.androidios.com/what-is-the-difference-between-satellite-navigation-systems-gps-and-glonass/*, 2014.